Journal for ImmunoTherapy of Cancer

CCR1 and CCR5 mediate cancer-induced myelopoiesis and differentiation of myeloid cells in the tumor

Serena Zilio ,[1] Silvio Bicciato ,[2] Donald Weed,[3] Paolo Serafini [1]

To cite: Zilio S, Bicciato S, Weed D, *et al*. CCR1 and CCR5 mediate cancer-induced myelopoiesis and differentiation of myeloid cells in the tumor. *Journal for ImmunoTherapy of Cancer* 2022;**10**:e003131. doi:10.1136/jitc-2021-003131

► Additional supplemental material is published online only. To view, please visit the journal online (http://dx.doi.org/10.1136/jitc-2021-003131).

Accepted 07 December 2021

[1]Department of Microbiology and Immunology, Sylvester Comprehensive Cancer Center, University of Miami, Miller School of Medicine, Miami, Florida, USA
[2]Department of Life Sciences, University of Modena and Reggio Emilia, Modena, Italy
[3]Department of Otolaryngology, Sylvester Comprehensive Cancer Center, University of Miami, Miller School of Medicine, Miami, Florida, USA

Correspondence to
Dr Paolo Serafini;
pserafini@miami.edu

ABSTRACT

Background Cancer-induced 'emergency' myelopoiesis plays a key role in tumor progression by inducing the accumulation of myeloid cells with a suppressive phenotype peripherally and in the tumor. Chemokine receptors (CCRs) and, in particular, CCR1, CCR2, CCR5, and CCR7 are emerging as key regulators of myeloid cell trafficking and function but their precise role has not been completely clarified yet because of the signal redundancy, integration, and promiscuity of chemokines and of the expression of these CCRs on other leukocyte subsets.

Methods We used the 4PD nanoparticle for the in vivo targeted silencing of CCR1, CCR2, CCR5, and/or CCR7 in the myeloid cells of tumor bearing mice to evaluate the effect of treatments on tumor growth, myeloid cell trafficking and polarization. We used flow and image cytometry and functional assays to monitor changes in the tumor microenvironment and depletion experiments and immune deficient mice to determine the role of $Ly6G^{+}$cells during tumor progression. We further evaluated in vitro the impact of chemokine receptor inhibition and tumor derived factors on myeloid cell differentiation from mouse and human hematopoietic stem and precursors cells (HSPCs) using flow cytometry, transcriptome analysis, cytokines beads arrays, functional assays, and mice deficient for CCR1 or CCR5.

Results 4PD-mediated in vivo silencing of CCR1 and CCR5 on myeloid cells and myeloid precursors was necessary and sufficient to inhibit tumor progression. Functional studies indicated that this antitumor effect was not mediated by alteration of myeloid cell chemotaxes but rather by the repolarization of polymorphonuclear myeloid-derived suppressor cells (MDSCs) into tumoricidal neutrophils. Transcriptome functional and cytokine analysis indicated that tumor derived factors induced CCL3 and CCL4 in HSPCs that, through the autocrine engagement of CCR1 and CCR5, induced HSPCs differentiation in MDSCs. These finding were confirmed across mice with different genetic backgrounds and using HSPCs from umbilical cord blood and peripheral blood of patients with cancer.

Conclusions Our data support the notion that CCR1 and CCR5 and their ligands are a master immunological hub activated by several tumor derived factors. Activation of this pathway is necessary for the differentiation of MDSCs and protumoral macrophages.

BACKGROUND

Myeloid cells in the tumor micro-environment and macro-environment can either promote or restrain tumor progression depending on their intrinsic polarization. Type-2 myeloid cells such myeloid-derived suppressor cells (MDSCs), inflammatory monocytes, and 'M2' macrophages promote immune exclusion and evasion, resistance to therapy, angiogenesis, and neoplastic cell proliferation and spreading, and are independent prognostic factors for overall survival in many human malignancies.[1–3] Conversely, type-1 myeloid cells can exert a direct tumoricidal activity, mediate the action of antibody therapies, and stimulate the adaptive antitumor immunity.[4–6] These cells are associated with better survival in some cancer types.[7 8] Thus, modulation of myeloid cell composition can have important repercussions on cancer progression and response to treatment.

Inflammatory chemokines such as CCL2, 3, 4, 5, 7, and 21, present in most human malignancies, modulate both neoplastic cell biology and the composition of tumor-infiltrating myeloid cells.[9] While the CCL2 receptor chemokine receptor (CCR)2 is the dominant receptor for recruiting myelomonocytic cells,[10] the CCL3 and CCL4 receptors CCR1 and CCR5 are also associated with MDSC accumulation,[11–14] and the CCL21 receptor CCR7 can promote the formation of intratumoral tolerogenic lymph node-like structures.[15] The dissection of the individual roles of CCR1, 2, 5, and 7, however, is hindered by the coexpression of these receptors in the same myeloid subsets,[16] by their capacity to bind to the same chemokine and to trigger similar intracellular signals,[17] and by the possible integration of downstream signaling pathways.[18] Each chemokine can bind multiple receptors and a receptor can be activated by different chemokines,

allowing for signal redundancy, robustness, integration, and synergy. This makes the understanding of their individual contribution to myeloid cells in tumor host function difficult.[19] Additionally, CCR 1, 2, 3, and 5 occupy a discrete and tight (165 kb) chromosomal locus (Chr9: 123962126–124127183 bp) and are expressed by most leukocyte subsets, making the in vivo study of their signal integration or redundancy difficult using the available mouse knock-out approaches.

To overcome these difficulties, we used the 4PD nanoplatform that targets tumor-infiltrating myeloid cells to determine the relative contributions of CCR1, 2, 5, and 7 silencing on myeloid cell function in tumor hosts.[20] Our study provides evidences for a synergistic and redundant role of CCR1 and 5 in mediating cancer-induced myelopoiesis and myeloid cell protumoral polarization. We show that tumor derived factors prime hematopoietic stem and precursors cells (HSPCs) to secrete CCL3 and 4 that promote HSPC differentiation into protumoral MDSCs via CCR1 and CCR5 signaling.

METHODS

All material and reagents are summarized in online supplemental table 1. Flow and image cytometry, qRT-PCR, CBA, cell isolation, and functional assays are described in online supplemental methods.

Cell lines

4T1, CT26, TSA, MCA203, DA3, A20, B16Lu8, HEK293, MDA-MB-231, cell lines were obtained from the American Type Culture Collection (ATCC), used within six passages from the original shipment, and maintained in complete media (online supplemental table 1) with 2-β-mercaptoethanol (20 µM). MDA-BoM-1833, and MDA231-LM2-4175 (a kind gift from Dr Lippman, University of Miami), 4T1HAThy1.1luciferase (a kind gift from Dr Borrello Johns, Hopkins University) were used within 10 passages from acquisition and maintained in complete media. B4B8 (a kind gift from Dr Thomas, University of Miami) were maintained in keratinocyte-SFM media supplemented with L-glutamine (2 mM), BPE (50 µg/mL) and EGF (5 pg/mL). Cells were annually tested via PCR for the presence of common pathogens and authenticated at the end of the project by STR analysis. Tumor conditioned media (TCM) was generated by admixing three parts of 0.2 µm filtered supernatant from the indicated cells (plated (3×10^6) 4 days early in T75 flask in 20 mL of complete media) with seven parts of complete media.

Human primary cells

Blood from patients (median age 59 years, range 49–72) with recurrent stage 3 or 4 head and neck squamous cell carcinoma (HNSCC) of the oral cavity or oropharynx undergoing salvage surgery were collected at the time of surgery. Umbilical cord blood (UCB) units from female and male newborn babies (2 days old) underwent Ficoll separation and red blood cell lysis.

Antagonists, shRNAs, and 4PD

B×471 and maraviroc (Sigma-Aldrich, 10 µM and 5 µM, respectively) were added to the culture on day 0 and 3. 4PD[20] (Kerafast) was complexed with short hairpin RNAs (shRNAs) (online supplemental table 1) at a 10:1 N/P–ratio following manufacturer instructions.

Mice and tumor experiments

8–10 weeks old BALB/c, C57BL/6J, and NSG mice were purchased from JAX laboratory, allowed to acclimate for at least 1 week, and maintained in the pathogen-free animal facilities at the University of Miami. Ear-tagged mice were randomized after tumor inoculation. BALB/c mice were injected orthotopically with the 3×10^5 4T1 cells, or subcutaneously (s.c.) with 5×10^5 CT26, 2×10^6 B4B8, or 5×10^5 TSA cells. C57BL/6 mice were injected s.c. with 5×10^5 MCA203 cells. Mice were injected intravenously three times a week with shRNAs (0.5 ug/g of each) loaded 4PD and euthanized when tumor reached ~1.2 cm of diameter or if signs of treatment or tumor related toxicity were evident as per IACUC guidelines. Tumors are expressed as volume (V)=L×S^2×0.52 where L is the largest diameter, and S is the perpendicular one.

$CCR5^{-/-}$C57BL/6, Cl4-Tg(TcraCl4,TcrbCl4)1Shrm/ShrmJ, and OT1-Tg(TcraTcrb)1100Mjb/J mice and $CCR1^{-/-}$C57BL/6 mice (a kind gift from Dr P Murphy, NIH) were bred in our facility. We used Cl4 and OT1 mice recognizing the K^d-restricted $HA_{518–526}$ peptide and the K^b restricted $OVA_{257–264}$ peptide, respectively, for suppressive assays. Depletion experiments were performed by intraperitoneally injection of the 1A8 rat-anti-mouse Ly6G antibody (10 µg/g) or IgG2a isotype control.

Tumor specimens

Mouse and human tumor specimens were processed within 1 hour from resection, cut in small pieces (~2×2 mm^2), washed two times with phosphate-buffered saline (PBS), incubated for 10–20' at 37°C with 5 volumes of PBS containing collagenase IV (10 mg/mL), $MgCl_2$ (100 µM), and $CaCl_2$ (100 µM), and minced by passing the mixture through a 3 mL needleless syringe every 10'. Reaction was stopped with 3 volumes of PBS-EDTA (2 mM), and cells were filtered with a cell-strainer and washed with PBS.

Statistics

All values depicted represent mean±SD of biological replica. Statistical tests (one-way, two-way, or three-way, analysis of variance (ANOVA) followed by Holm-Sidak or Bonferroni test for multiple pairwise comparison or Student's t-test) were applied in a two-sided, unpaired fashion after normality was evaluated by the Shapiro-Wilk test. ANOVA on ranks followed by Tukey test for multiple comparison was used for those data that failed the normality test. The variance was similar between experimental groups in each experiment unless otherwise stated.

In vitro analyses and in vivo experiments were repeated two to five times to ensure reproducibility and cumulative data are shown. Log-rank test was used for survival analysis followed by pairwise multiple comparison procedures (Holm-Sidak method). No experimental data point was excluded from analysis. Sample size was determined by power analysis using effect size determined by pilot experiments or prior experience of the authors. Statistical analyses were performed with Sigmaplot.

Study approval

All animal experiments were conducted under a protocol approved by the Division of Veterinary Resources and the Institutional Animal Care & Use Committee of the University of Miami.

RESULTS

The 4PD nanoplatform allows to simultaneously silence multiple chemokine receptors *in vivo*

qRT-PCR analysis of $CD11b^+$cells from the tumor or the spleen of 4T1 bearing mice indicates that CCR1, 5 and 7 are significantly upregulated at the tumor whereas CCR2 is highly expressed on myeloid cells from both tissues (online supplemental figure 1). To understand the role of these receptors on myeloid cell composition and function at the tumor site, we employed the previously characterized 4PD nanoplatform to silence in vivo CCR1, 2, 5 and 7.[20] On injection in BALB/c mice bearing the 4T1 carcinoma, this nanoparticle recognized preferentially ($p<0.001$) tumor-infiltrating myeloid cells as determined by three way-ANOVA using tissues, leukocyte subsets ($CD45^-$ vs $CD45^+CD11b^-$ vs $CD45^+CD11b^+$), and treatment as factors. Further analysis revealed that 4PD accumulated mostly on tumor-infiltrating polymorphonuclear (PMN)-MDSC ($p<0.001$). In sharp contrast, the control dendrimer conjugated with random peptides were less specific (figure 1A). Interestingly, we observed also 4PD binding to lineage negative $CD34^+ckit^+$ hematopoietic precursors in the bone marrow, spleen and tumor suggesting that this platform might be used to modulate gene expression on HSPCs. We repeated the experiment in the C57BL/6 MCA203 fibrosarcoma model characterized by fewer MDSCs in the spleen and in the tumor. In this setting as well, 4PD showed a preferential binding to myeloid cells ($p=0.003$) in all tissues evaluated. As we previously showed in the B16 model, in the MCA203 model, 4PD bound preferentially monocytic MDSCs (mMDSCs) ($p<0.001$) in both spleen and tumor. This can be explained by the heterogeneity of myeloid cell subsets across tumor models and mice strains.[20] Also in the MCA203 model, 4PD recognized HSPCs-like cells and, in particular, cells resembling multipotent progenitors (MPPs) and granulocyte-monocyte progenitors (GMPs) in the spleen and MPP-like cells in the tumor (figure 1B).

We then evaluated the ability of the 4PD nanoplatform to silence multiple CCRs in myeloid cells in time course experiments. To this aim, we injected 4PD loaded with an equimolar mixture of shRNAs against CCR1, 2, 5, and 7 intravenously to 4T1 tumor bearing mice. This treatment silenced these genes for 3–4 days in tumor-infiltrating myeloid cells but not in the splenic counterpart (figure 1C) nor in CD11b negative cells (not shown).

Simultaneous silencing of CCR1 and CCR5 on myeloid cells in vivo inhibits tumor progression

Once the capacity of 4PD to bind and transfect myeloid cells in vivo with multiple shRNAs was determined, we evaluated the effect of chronic CCR1, CCR2, CCR5, and CCR7 silencing on tumor progression. Systemic administration of 4PD loaded with shRNAs specific for CCR1, 2, 5 and 7 to 4T1 bearing mice significantly ($p<0.001$) delayed tumor progression and decreased the number of lung metastases, whereas the corresponding scrambled shRNAs (SCR1, 2, 5, and 7) had no effect (figure 2A). To evaluate which CCRs were responsible for the antitumor effect, 4T1 bearing mice were given 4PD loaded with shRNAs against: (i) CCR1, 2, 5, and 7, (ii) scrambled shRNA1, CCR2, 5, and 7, (iii) CCR1, scrambled shRNA2, CCR5 and 7, (iv) CCR1 and 2, scrambled shRNA5, and CCR7, (v) CCR1, 2, and 5 and scrambled shRNA7 or (vi) scrambled shRNAs1, 2, 5 and 7. Again, simultaneous silencing of all four CCRs resulted in an important antitumor effect that was lost when either CCR1 or CCR5 were omitted from the shRNA mixture. In contrast, the absence of CCR2 or CCR7 shRNAs did not impair the therapeutic effect (figure 2B). Then, we evaluated whether silencing of CCR1 and/or CCR5 was sufficient to inhibit tumor growth (figure 2C). While silencing of either CCR1 or CCR5 gave modest results, silencing both receptors significantly ($p<0.001$) reduced tumor size. We observed no effect when mice were treated with scrambled shRNAs. To determine whether this effect was reproducible in other models, we challenged mice with the 4T1 tumor, the TSA breast carcinoma, the CT26 colon carcinoma, the B4B8 squamous cell carcinoma (figure 2D), or the MCA203 fibrosarcoma. Once tumors become palpable, mice were treated with shRNAs against CCR1 and 5. In all these models, chronic targeted silencing of CCR1 and CCR5 significantly reduced tumor growth and the lung metastases in the 4T1 model (online supplemental figure 2). Interestingly, in the slow growing B4B8 carcinoma, treatment induced tumor rejection in approximately 60% of the mice.

Finally, we evaluated whether CCR1 and CCR5 blockade inhibited myeloid cell trafficking to the tumor (figure 2E). Briefly, we divided splenocytes from 4T1 bearing mice in two aliquots. One was pulsed with maraviroc and B×471 (specific antagonists of CCR5 and CCR1, respectively) and labeled with CellTrace Far Red dye, the other one was left unpulsed and labeled with Carboxy Fluorescein Succinimidyl Ester(CFSE). The two aliquots were admixed at one to one ratio and injected intravenously in 4T1 bearing mice. Two hours later, we evaluated the biodistribution of donors' $CD3^+$ and $CD11b^+$ leukocytes by flow cytometry. While pretreatment with CCR1 and

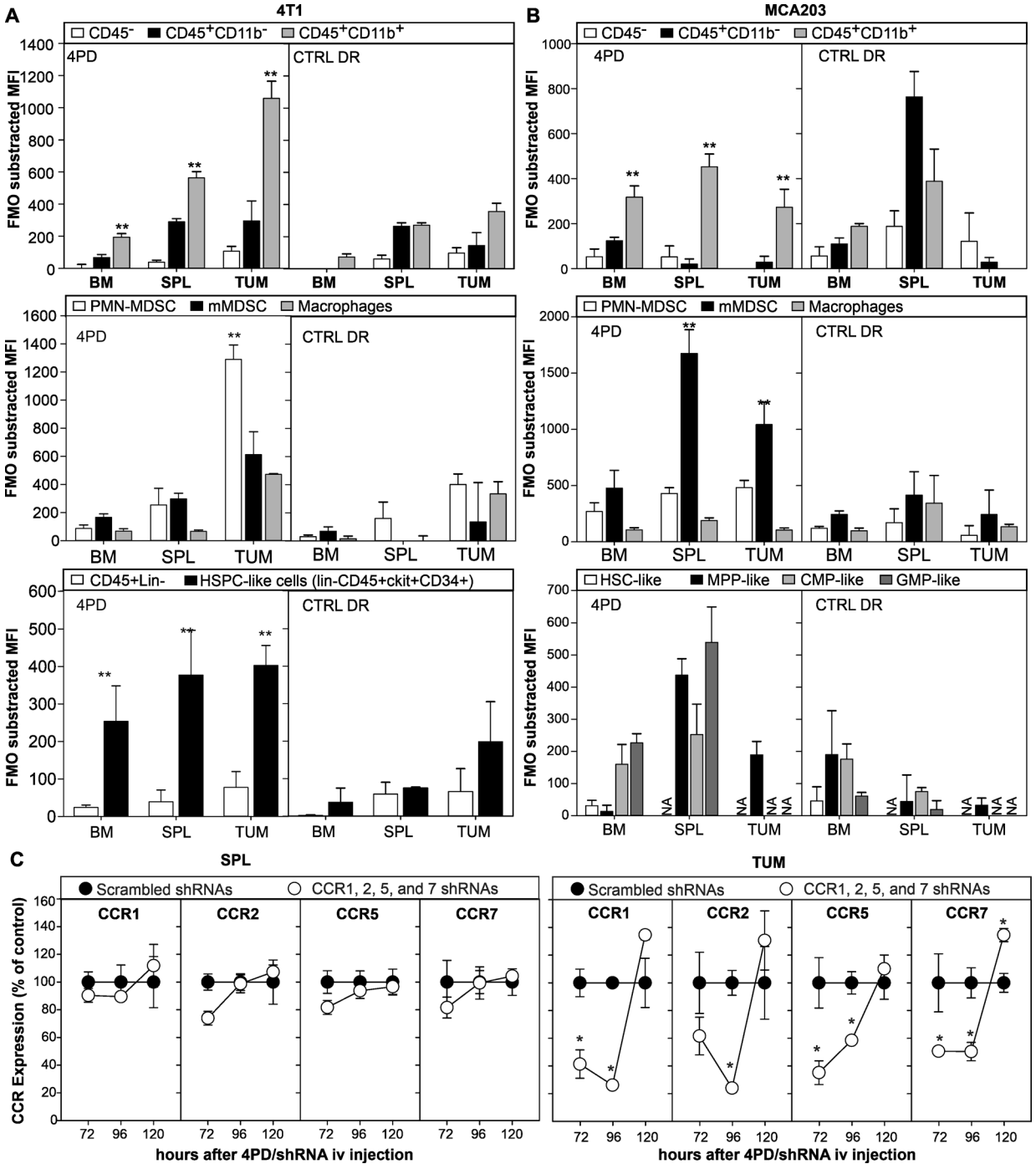

Figure 1 4PD allows the simultaneous targeted silencing of multiple chemokine receptors. BALB/c (A) or C57BL/6 (B) mice were challenged with the 4T1 mammary carcinoma orthotopically or the MCA203 fibrosarcoma subcutaneously, respectively. When tumor reached approximately 0.5 cm in diameter, mice were injected intravenously with 4PD loaded with AF555 siRNA. Two hours later, 4PD binding to the indicated myeloid subsets was evaluated in the bone marrow, spleen, and tumor by flow cytometry. **P<0.001 in Bonferroni multiple comparison test across leukocyte subsets in each tissue post three-way ANOVA using tissue, leukocyte subset and treatment as factors. (C) 4T1 bearing BALB/c mice were injected intravenously with 4PD loaded with an equimolar mixture of shRNAs specific for CCR1, CCR2, CCR5, and CCR7. Expression of these chemokine receptors was evaluated by qRT-PCR at the indicated time on CD11b$^+$cells isolated from tumors and spleens. **P<0.001 in two-way ANOVA vs control. ANOVA, analysis of variance; CCR, chemokine receptors; iv, intravenous; mMDSC, monocytic MDSC; MDSC, polymorphonuclear myeloid-derived suppressor cell; shRNA, short hairpin RNA; siRNA, small inhibitory RNA.

CCR5 antagonists significantly reduced the T cell chemotaxes to the lungs, spleen, and tumor, we did not observe any difference on the biodistribution of CD11b$^+$ myeloid cells (figure 2E). This argues against a role of CCR1 and CCR5 on myeloid cell trafficking to the tumor. These data suggest that CCR1 and CCR5 signaling in myeloid cells promotes tumor progression by a mechanism that might be unrelated to their migration.

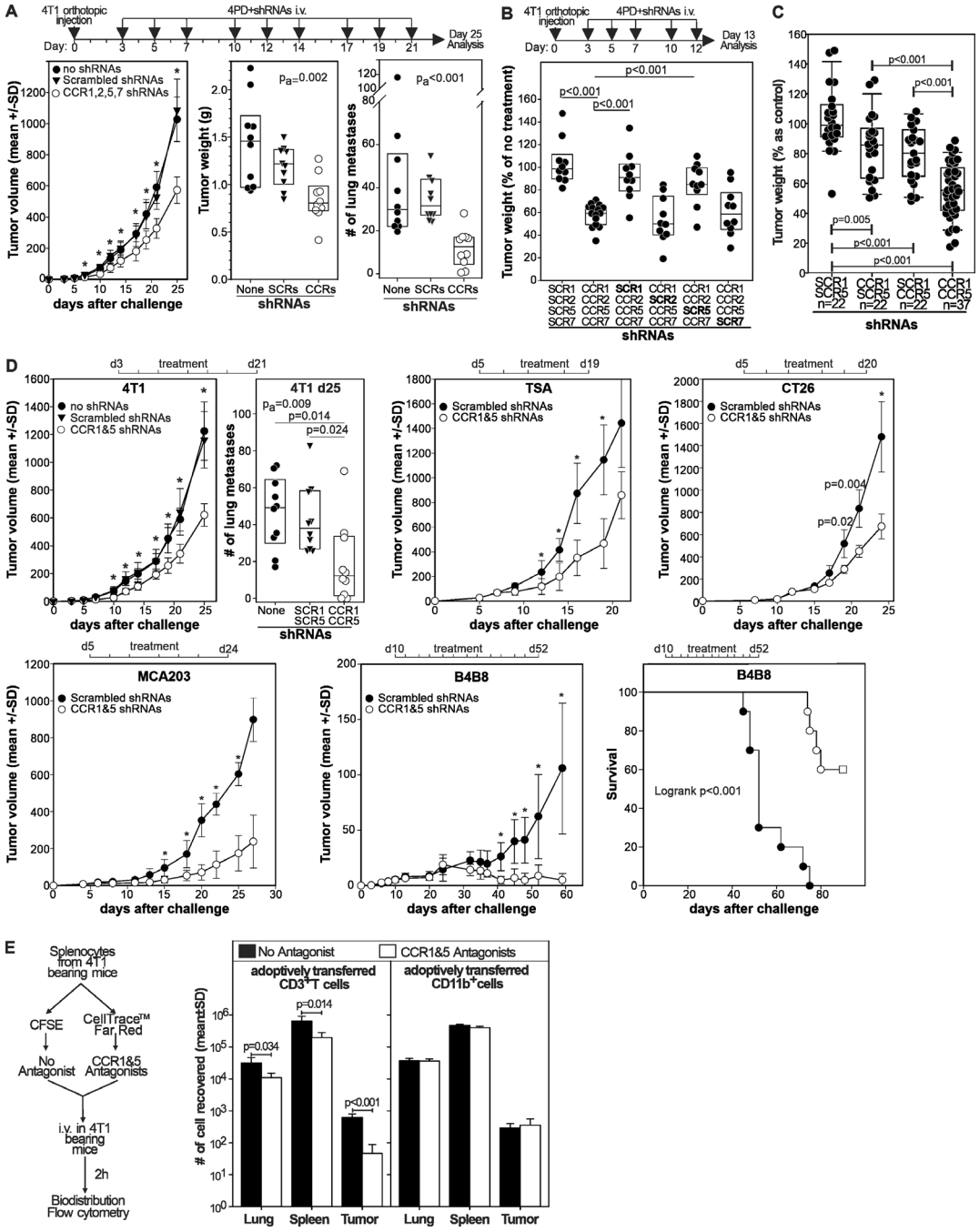

Figure 2 Targeted CCR1 and CCR5 silencing limits tumor progression by chemotaxis independent mechanisms. (A) BALB/c mice (n=10) were injected orthotopically with the 4T1 mammary tumor and, starting 3 days after challenge, treated three times a week with 4PD loaded with the indicated shRNAs. Twenty-five days after challenge mice were euthanized primary tumors weighted and lung metastases counted. Data are cumulative of two independent experiments (B) mice (n=10–16) treated as in (A) were euthanized 13 days after challenge and tumor weighted. Data are cumulative of three independent experiments and expressed as percentage of control (untreated 4T1 bearing mice). (C) Mice (n=22–37), challenged 3 days before with 4T1 cells, were intravenously treated three times a week with 4PD loaded with (i) scrambled shRNAs, (ii) CCR1 and scrambled$_{CCR5}$ shRNAs, (iii) CCR5 and scrambled$_{CCR1}$ shRNAs, or (iv) CCR1 and CCR5 shRNAs. Tumor weight was measured 13 days after challenge. Data are cumulative of five independent experiments. (D) Mice (n=10) bearing the indicated tumors were treated intravenously three times a week with 4PD loaded with the indicated shRNAs. Tumor progression was followed. Significant differences were evaluated by two-ways ANOVA using 'time' and 'treatment' as factors. *=P<0.001 within each time point in a post-hoc Holm-Sidak test for multiple pairwise comparison. Data derived from two independent experiments in each model. (E) Splenocytes from 4T1 tumor bearing mice were divided in two aliquots and either labeled with CellTrace Far Red and pulsed with maraviroc and B×471 or labeled with CFSE and left untreated. 10^7 cells from a 1:1 mixture of the two aliquots were injected intravenously in 4T1 bearing recipient mice. Transferred CellTrace Far Red$^+$ (antagonists) or CSFE$^+$ (no antagonists) cells were enumerated among the CD3$^+$ or CD11b$^+$ leukocytes by flow cytometry 2 hours after injection. ANOVA, analysis of variance; CCR, chemokine receptors; CFSE, Carboxy Fluorescein Succinimidyl Ester; shRNA, short hairpin RNA.

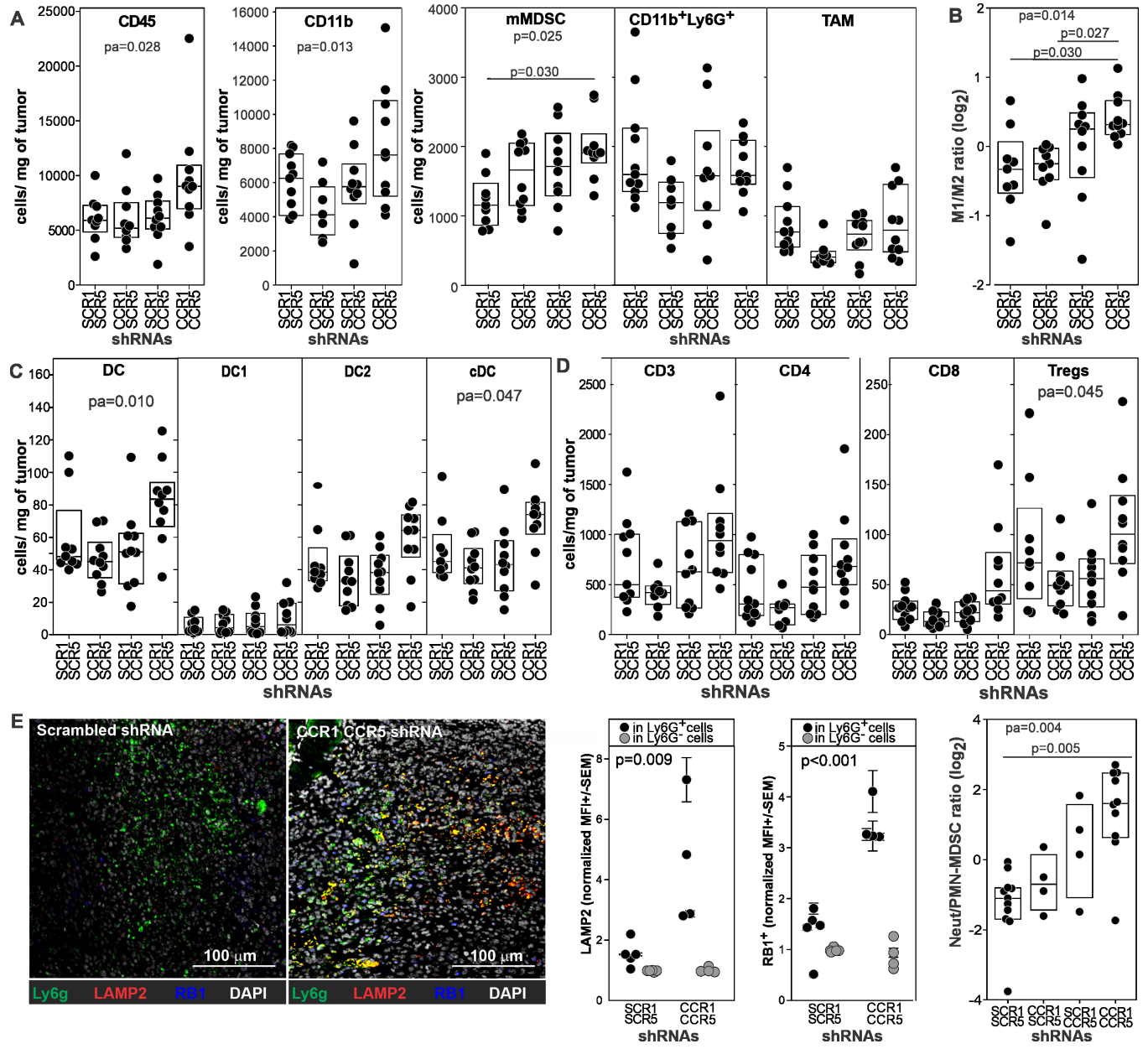

Figure 3 Targeted CCR1 and CCR5 silencing modulates the tumor microenvironment. Tumors from 4T1 bearing mice (n=10) treated with 4PD loaded with (i) scrambled shRNAs, (ii) CCR1 and scrambled$_{CCR5}$ shRNAs, (iii) CCR5 and scrambled$_{CCR1}$ shRNAs, or (iv) CCR1 and CCR5 shRNAs were analyzed by multicolor flow cytometry and data reported as cell density. Gating strategies are depicted in online supplemental figure 2. (A) Myeloid subsets. (B) M1/M2 macrophage ratio. (C) DC subsets. (D) T cell subsets. (E) Tumor sections from the mice (n=5) treated with scrambled or CCR1 and CCR5 shRNAs were stained with DAPI (white) and antibodies against Ly6G (green), Lysosomal Associated Membrane Protein 2 (red) and retinoblastoma 1 (blue), scanned, and analyzed by image cytometry. CCR, chemokine receptors; cDC, conventional dendritic cell; shRNA, short hairpin RNA.

CCR1 and CCR5 silencing alters myeloid cell phenotype in the tumor microenvironment

Since CCR1 and CCR5 targeted silencing mediates a significant antitumor effect, we evaluated its action on the tumor microenvironment (figure 3). We treated 4T1 bearing mice with 4PD loaded with shRNA against CCR1 and/or CCR5 or corresponding scrambled shRNAs as control. Thirteen days after challenge, we characterized the tumor microenvironment by flow and image cytometry and tested myeloid cells functionally in suppressive and tumor co-culture assays. Flow cytometry (online supplemental figure 3) showed that silencing of both CCR1 and CCR5 slightly increased the intratumoral density of CD45$^+$leukocytes and CD11b$^+$myeloid cells whereas did not change the number of macrophages, mMDSCs, and CD11b$^+$Ly6G$^+$ populations (figure 3A). Analysis of Tumor associated macrophage (TAM) subsets using the major histocompatibility complex (MHC) class II and CD206 markers revealed a significant (p=0.014) change in the polarization of this subset toward a M1-like

phenotype (figure 3B) and a modest increase (p=0.010) in the concentration of dendritic cells (DCs) and conventional (c)DCs (p=0.047) in particular (figure 3C). Surprisingly, we did not observe changes in the density of the overall lymphocyte nor in the CD4 and CD8 subsets (figure 3D), arguing against a prominent role of T cells in the observed antitumor effect. We observed no changes when only either of the chemokine receptors was silenced (figure 3).

Since $CD11b^+Ly6G^+$ cells are the largest myeloid subset in this model and they include both 'classical' antitumoral neutrophils (NeuT) and protumoral PMN-MDSCs,[21] that cannot be easily resolved by flow cytometry, we evaluated their phenotype by image cytometry (figure 3E and online supplemental figure 4) using antibodies against Ly6G, Lysosomal Associated Membrane Protein 2 (LAMP2), and retinoblastoma (RB1). While Ly6G identified both PMN-MDSCs and neutrophils, LAMP2 and retinoblastoma allow the discrimination of these two polymorphonuclear subsets.[22] $Ly6G^+$ cells in the tumor of control mice were mostly RB1 and LAMP2 negative (figure 3E) suggesting a PMN-MDSC phenotype.[22] In sharp contrast, $Ly6G^+$ cells in the tumor of mice silenced for CCR1 and CCR5 had a high expression of RB1 and LAMP2 consistent with a 'classical' neutrophil phenotype. Taken together, these data suggest that targeted inhibition of CCR1 and CCR5 on myeloid cells alters the tumor microenvironment by reducing the number of PMN-MDSCs and M2 macrophages and by increasing the concentration of cells with a phenotype consistent with classical neutrophils.

CCR1 and CCR5 targeted silencing changes the function of tumor-infiltrating myeloid cells

Having observed the changes in the tumor-infiltrating PMNs, we performed functional assays to determine if these changes translated into differences in myeloid cell suppressive or tumoricidal activity. We purified $CD11b^+$ myeloid cells from the spleen and the tumor of mice treated with CCR1 and CCR5 shRNAs or with scrambled shRNAs and tested their suppressive activity against HA specific, $CD8^+$ T cells stimulated with the relevant peptide. While splenic $CD11b^+$ from the different groups were equally suppressive, $CD11b^+$ cells from the tumor of mice treated with CCR1 and CCR5 shRNAs showed a reduced suppressive activity (figure 4A).

To evaluate myeloid cell tumoricidal activity, we co-cultured $CD11b^+$ cells from treated mice with 4T1-luciferase cells and enumerated neoplastic cells 18 hours later by luciferase assay (figure 4B). While tumor-infiltrating myeloid cells from control mice did not affect neoplastic cell number, $CD11b^+$ cells from CCR1 and CCR5 shRNA treated mice drastically reduced the number of 4T1 cells in culture indicating a tumoricidal action.

Since most of the phenotypic changes in the tumor-infiltrating leukocytes occurred in the polymorphonucleate subset that is also the most prominent population in the 4T1 model, we assessed the effect of $Ly6G^+$cell depletion in 4T1 bearing mice undergoing 4PD treatment with shRNAs specific for CCR1 and CCR5 or scrambled shRNAs as control (figure 4C). In mice treated with the isotype control, CCR1 and CCR5 targeted silencing significantly reduced tumor progression compared with the PBS control. Notably, depletion of $Ly6G^+$ cells drastically reduced the antitumor activity of CCR1 and CCR5 shRNAs. Conversely, in mice treated with scrambled shRNAs, Ly6G depletion reduced tumor progression whereas we observed no differences from the PBS control in the mice treated with the isotype antibody (figure 4C).

Finally, we used NSG mice to evaluate the possible contribution of B, T and natural killer (NK) cells in the observed antitumor effect. Briefly, BALB/c or NSG mice were challenged with the 4T1 tumor orthotopically and treated intravenously with 4PD loaded with scrambled or CCR1 and CCR5 shRNAs 3, 5, 7, 10 and 12 days after challenge. As observed above, CCR1 and CCR5 targeted silencing significantly inhibited tumor growth in BALB/c mice (figure 4D). A similar antitumor effect was observed also in the NSG mice indicating that T, B, and NK cells have minimal or no effect on the antitumor activity mediated by CCR1 and CCR5 targeted silencing.

Taken together, these data indicate that silencing of CCR1 and CCR5 on myeloid cells changes their function from suppressive to antitumoral and highlight the role of neutrophils in the observed antitumor effect.

CCR1 and CCR5 blockade promotes the differentiation of tumoricidal neutrophils

Since HSPC-like cells are found in the cancer host in the periphery and intratumorally (online supplemental figure 5A), express CCR1 and CCR5 (online supplemental figure 5B), and can be transfected by 4PD (figure 1), we evaluated whether CCR1 and CCR5 blockade can affect the differentiation of HSPC-like cells into MDSCs. We isolated intratumoral $CD45^+$ Lineage negative hematopoietic precursors from 4T1 bearing mice and cultured them with 4T1 TCM in the presence or absence of the CCR1 and CCR5 antagonists B×471 and maraviroc, respectively (figure 5A). In cultures treated with vehicle, TCM induced the differentiation of macrophages, mMDSCs, FSC-A^{high} PMN-MDSCs, and few classical FSC-A^{low} neutrophils supporting the notion that intratumoral HSPC-like cells can differentiate into more mature myeloid cells. Simultaneous blockade of CCR1 and CCR5 inhibited macrophages, mMDSCs, and PMN-MDSCs differentiation and promoted the differentiation of 'classical' FSC-A^{low} neutrophils. To understand if CCR1 and CCR5 blockade modulates not only the phenotype but also the function of myeloid cells induced by tumor derived factors, we employed bone marrow cells from naïve mice. We cultured BM cells with 4T1 TCM with or without CCR1 and CCR5 antagonists (figure 5B) for 4 days and then characterized the resulting populations by flow cytometry. As expected, in the absence of the antagonists, TCM differentiated BM cells largely in $CD11b^{int}$ FSC-A^{high} $Ly6G^+$PMN-MDSCs, $CD11b^{high}$ $Ly6C^+$ mMDSCs, with few contaminations of $Ly6G^-Ly6C^-F4/80^+$ macrophages

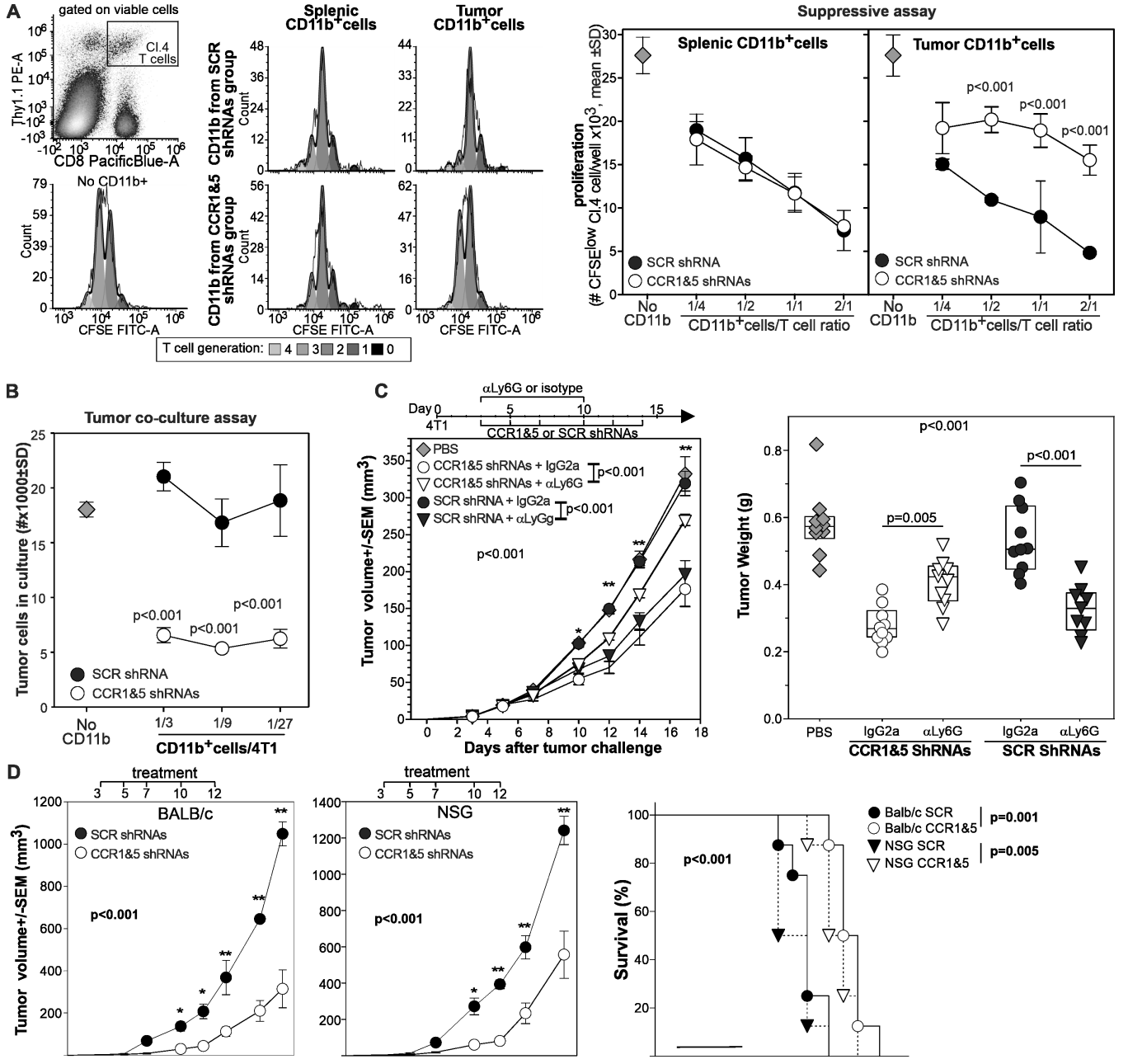

Figure 4 In vivo silencing of CCR1 and CCR5 changes the function of tumor-infiltrating myeloid cells from immunosuppressive to tumoricidal. (A) CD11b$^+$cells from the spleen or tumor of 4T1 bearing mice treated with scrambled or CCR1 and CCR5 shRNAs were incubated with HA-specific, CFSE-labeled T cells stimulated with the relevant peptide. Proliferation was evaluated 3 days later by flow cytometry, the number of proliferating clonotypic T cells per well is reported. (B) CD11b$^+$cells from the tumor of mice treated with scrambled or CCR1 and CCR5 specific shRNAs were incubated at different ratio with 4T1-luciferase cells. Neoplastic cell number was evaluated 24 hours later by luciferase. *=P<0.001. (C) 4T1 bearing mice (n=10) were treated intravenously with shRNAs against CCR1 and CCR5 or scrambled shRNAs and treated with either rat anti-Ly6G depleting antibody or isotype control as depicted. Tumor progression was monitored, and tumor weight measured 18 days after challenge. (D) BALB/c or NSG mice (n=8/group) were injected orthotopically with 4T1 tumor and treated intravenously with 4PD loaded with scrambled or CCR1 and CCR5 shRNAs as indicated. *: P<0.01; **p<0.001. CCR, chemokine receptors; CFSE, Carboxy Fluorescein Succinimidyl Ester; HA, hemagglutinin; shRNA, short hairpin RNA.

and CD11b^{high} FSC^{low} Ly6G$^+$neutrophils. Conversely, in the presence of maraviroc and B×471 TCM induced the differentiation of large number of classical neutrophils, increased the number of macrophages, and drastically reduced both mMDSCs and PMN-MDSCs (figure 5B). We then cultured FACS sorted Ly6G$^+$ or Ly6C$^+$ cells differentiated in the presence or absence of CCR1 and CCR5 antagonists with 4T1-luciferase cells (figure 5C). Compared with the 4T1 seeded alone, the addition of Ly6G$^+$cells from the control cultures induced a higher recovery of 4T1 cells supporting the notion that PMN-MDSCs promote neoplastic cell proliferation. In sharp

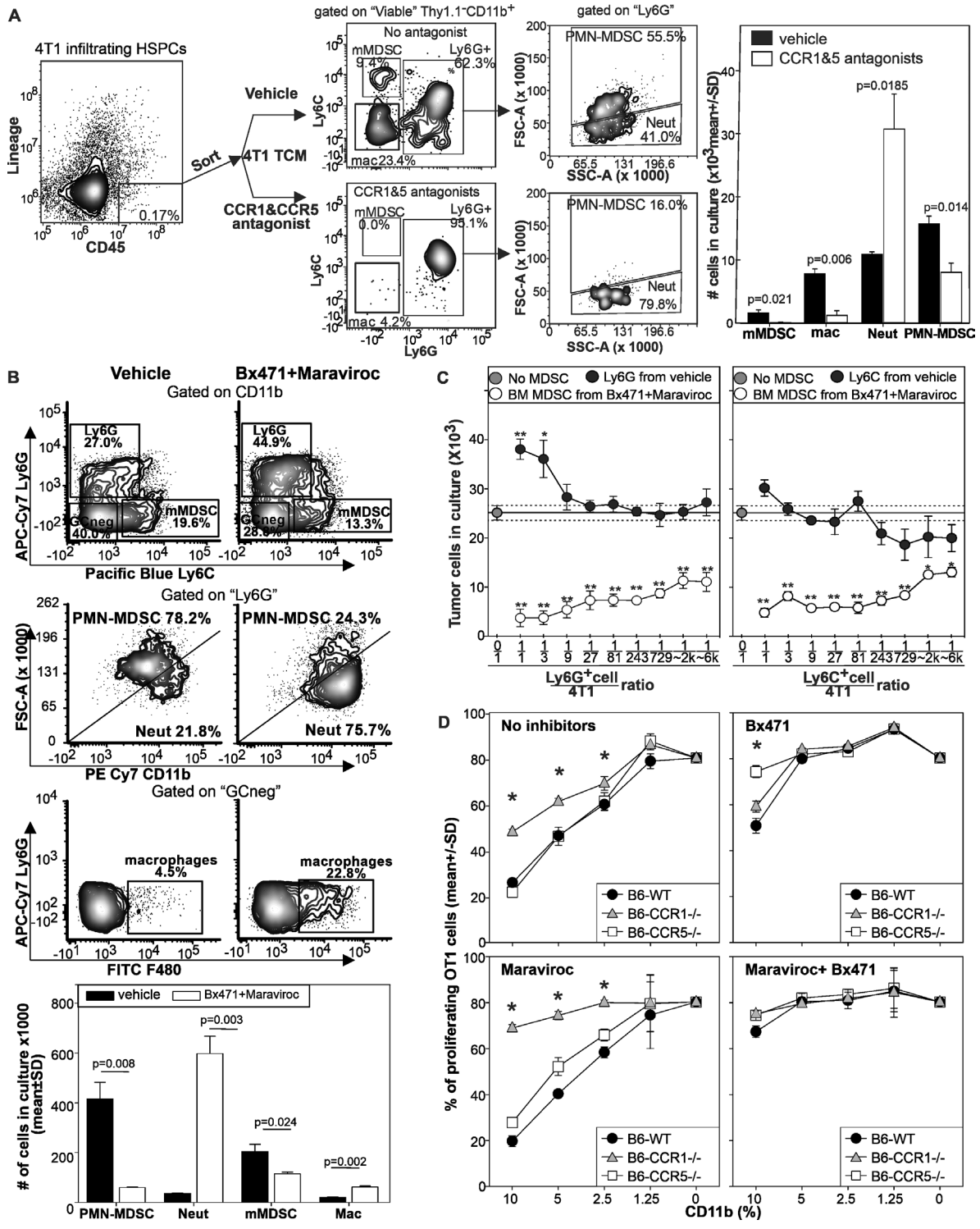

Figure 5 CCR1 and CCR5 regulate HSPC commitment toward MDSCs or tumoricidal neutrophils. (A) Lin-/CD45$^+$cells were sorted by FACS from pooled tumors of 14 mice injected 20 days before with 4T1. Sorted cells (5×10^4) were stimulated by 4T1-TCM in the presence or in the absence of maraviroc and B×471 and enumerated by flow cytometry 4 days later. Data derived from two independent experiments. (B) BALB/c BM cells were cultured with 4T1-TCM and: (i) maraviroc, (ii) B×471, (iii) both antagonists, or (iv) vehicle for 4 days and characterized by flow cytometry. (C) FACS sorted CD11b$^+$Ly6G$^+$ or CD11b$^+$Ly6C$^+$cells from the cultures were incubated with 4T1-luc cells at the indicated ratio. (D) BM cells from naive CCR1$^{-/-}$, CCR5$^{-/-}$ or CCR1$^{+/+}$ CCR5$^{+/+}$ C57BL/6 mice were stimulated by MCA203 TCM with maraviroc, B×471, both antagonists, or vehicle. 4 days later, cells were magnetically purified and tested in suppressive assays against OT1 cells stimulated with the relevant peptide. *p<0.01, **p<0.001. CCR, chemokine receptors; HSPCs, hematopoietic stem and precursors cells; PMN-MDSC, polymorphonuclear myeloid-derived suppressor cell; TCM, tumor conditioned media; WT, wild type.

contrast, Ly6G$^+$ cells differentiated with maraviroc and B×471 dramatically decreased 4T1 recovery suggesting a strong and direct tumoricidal action. Similar results were observed with Ly6C$^+$cells (figure 5C). To further test the involvement of CCR1 and CCR5 in MDSC differentiation, we employed bone marrow from CCR1$^{-/-}$, CCR5$^{-/-}$, or wild type (WT) C57BL/6 mice (figure 5D). As expected, MCA203-TCM drove BM cells from WT mice to differentiate into highly suppressive MDSCs. We observed a slight reduction in MDSC suppressive activity when CCR1$^{-/-}$BM cells were differentiated with no antagonists, whereas no differences in suppressive activity were evident with CD11b$^+$cells differentiated from CCR5$^{-/-}$BM. Addition of the CCR1 antagonist B×471 during differentiation had low effect on CCR1$^{-/-}$BM-derived CD11b$^+$ cells, it partially reversed the suppressive activity of WT-BM derived myeloid cells, and completely reversed the suppressive activity of CCR5 deficient myeloid cells. Conversely, maraviroc during MDSC differentiation reversed the suppressive activity of myeloid cells from CCR1 deficient BM-cells but had no effect on MDSCs differentiated from the BM of WT or CCR5$^{-/-}$ mice. The combined use of both B×471 and maraviroc during differentiation completely inhibited the suppressive activity of myeloid cells differentiated from all the genetic backgrounds.

Neutrophils have been proposed to exert their tumoricidal action via degranulation and or secretion of nitric oxide, lysozyme, superoxide or neutrophil extracellular traps (NETs).[23–26] To explore if any of these pathways was involved in neutrophil's tumoricidal action we performed tumor co-culture assays in the presence of 4,4′-Diisothiocyanatostilbene-2,2′-disulfonic acid disodium salt to inhibit NETosis and degranulation, N,N′,N″-Triacetylchitotriose to inhibit lysozyme, recombinant superoxide dismutase to neutralize superoxide, imidazole to inhibit the respiratory burst, or N^G-Methyl-L-arginine to inhibit nitric oxide synthase 2. None of the tested inhibitors reversed neutrophil tumoricidal activity (online supplemental figure 6).

These results support the notion that CCR1 and CCR5 silencing modulates tumor driven differentiation of myeloid precursors by inhibiting MDSC polarization and increasing the number of myeloid cells that induce tumor death by a yet undisclosed mechanism.

CCR1 and CCR5 signaling mediates the protumoral changes induced in HSPCs by tumor derived factors

Because of the absence of suitable markers that allow the easy discrimination of PMN-MDSCs from 'classic' neutrophils, we employed transcriptome analysis to determine the phenotype of myeloid cells differentiated by TCM with or without CCR1 and CCR5 antagonists. We cultured BM cells for 24 hours in RPMI media (RPMI) or in TCM in the presence or absence of B×471 and maraviroc (TCM+CCR antagonists). We hybridized the RNA isolated from sorted CD11b$^+$ cells on gene expression microarrays and we merged gene expression profiles with publicly available transcriptional data of CD11b$^+$ cells from 4T1 tumors and from BM (BM CD11b$^+$) and spleen (splenic CD11b$^+$) of naïve BALB/c mice (figure 6 and online supplemental table 2). Next, we performed an unsupervised hierarchical clustering analysis of gene expression profiles. BM cells incubated with 4T1-TCM grouped with tumor-infiltrating myeloid cells, BM cells cultured in RPMI media clustered with splenic CD11b$^+$ cells, and BM cells cultured with TCM and CCR1 and CCR5 antagonists associated with CD11b$^+$ cells from the BM of naïve mice (figure 6A). Next, we investigated the effect of CCR1 and CCR5 antagonists on the transcriptional levels of genes previously associated with PMN-MDSCs, with M1 or M2 macrophages, or with classical neutrophils (figure 6B and online supplemental table 3). As expected, compared with RPMI, TCM upregulated several genes associated to the PMN-MDSC phenotype, suppressive activity, or differentiation (PMN-MDSC, red in figure 6B), and/or a M2 macrophages (purple in figure 6B). Conversely, the CCR1 and CCR5 blockade inhibited the expression of most of these genes and promoted the upregulation of genes associated with classical neutrophils (Neut, light green figure 6B) or M1 macrophages (dark green figure 6B) including lactostranferrin, a glycoprotein with known antitumoral activity.[27] Functional enrichment analysis showed that B×471 and maraviroc inhibited the activation of metabolic (eg, oxidative phosphorylation response, hypoxia) and signaling pathways (eg, interleukin (IL)6-STAT3, mTORC1) associated with MDSCs and induced by TCM in BM cells (online supplemental figure 7).

Since MDSCs can be differentiated in the absence of exogenous CCR1 and CCR5 ligands (eg, by using GM-CSF and IL6),[28] we evaluated whether TCM upregulates CCR1 and CCR5 ligands. This analysis revealed that the CCR1 and CCR5 ligands CCL3 and CCL4 were among the most significantly upregulated genes (figure 6C).

We next evaluated whether CCL3 and CCL4 induction was a widespread phenomenon or whether it was only associated to the 4T1 tumor. To this aim, we measured CCL2, CCL3, CCL4, and CCL5 by CBA in TCM from different cancer types or in cultures of BM cells stimulated with the same TCMs or with recombinant cytokines involved in MDSC differentiation (figure 6D and online supplemental figure 8). At baseline, we detected elevated concentrations of CCL2 and CCL5 but low concentrations of CCL3 and CCL4 in most TCMs (online supplemental figure 8A). After 24 hours with TCM stimulation or recombinant cytokines involved in MDSC differentiation, BM cultures significantly increased concentrations of CCL3 and CCL4 (range 5–490 and 7–1648 folds for CCL3 and CCL4, respectively) (figure 6D). Recombinant GM-CSF, secreted by most mouse and human tumors,[29] stimulated both CCL3 and CCL4 (figure 6D). TCM stimulation or any recombinant cytokine tested did not modulate CCL2 or CCL5 (online supplemental figure 8B). Intracellular staining confirmed that almost half of HSPCs secrete CCL3 and CCL4 on stimulation with 4T1 TCM or GM-CSF +IL6a combination commonly used to differentiate MDSCs (figure 6E).[28] A similar analysis

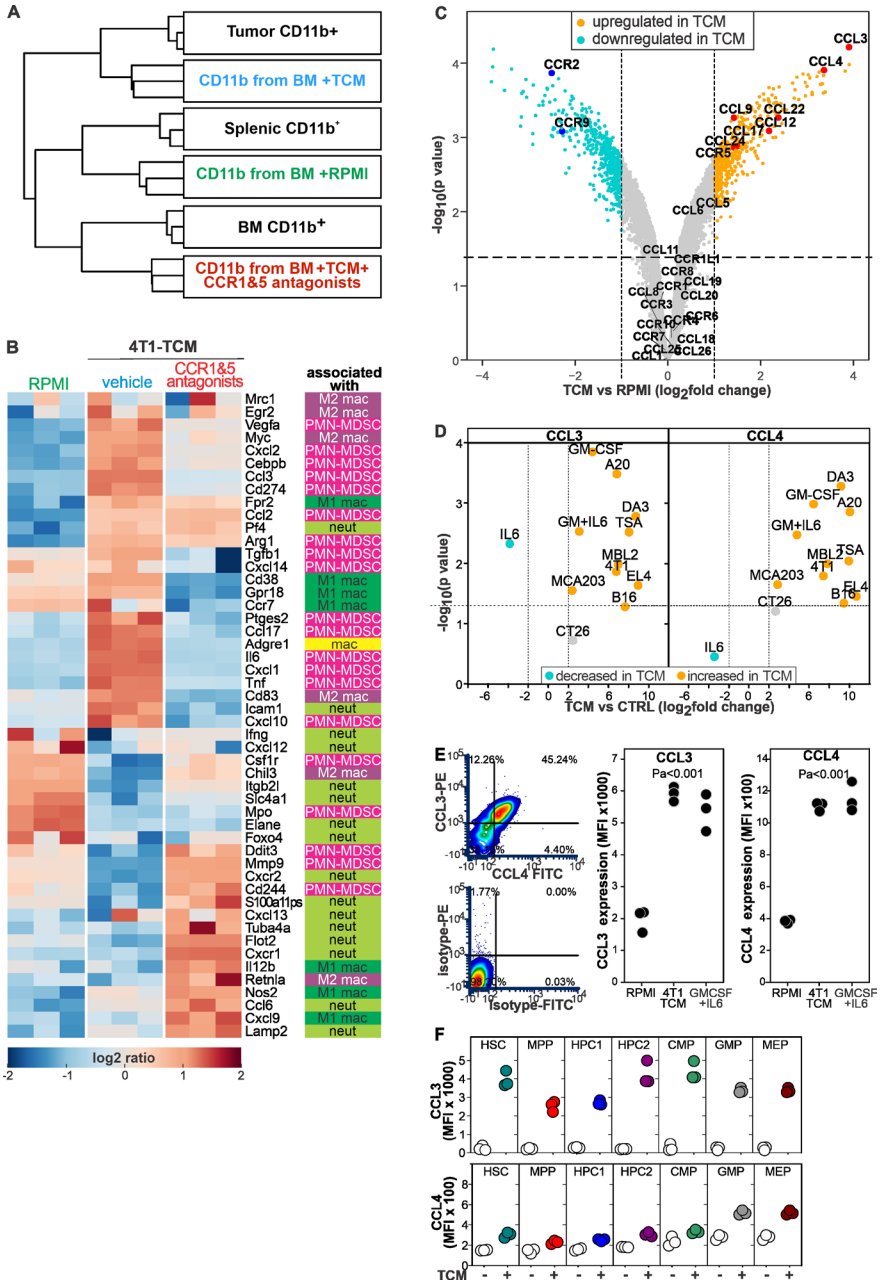

Figure 6 Tumor derived factors induce MDSC commitment via secretion of CCL3 and CCL4 and CCR1 and CCR5 signaling. BALB/c BM cells were cultured in RPMI or 4T1-TCM supplemented with B×471 and maraviroc or with vehicle. Twenty-four hours later, CD11b$^+$cells were magnetically isolated, RNA extracted and hybridized on Affymetrix microarrays. (A) Gene expression data of CD11b$^+$cells were merged with publicly available transcriptional profiles of CD11b$^+$cells isolated from 4T1 tumors or from the BM (BM CD11b$^+$) or the spleen (splenic CD11b$^+$) of naïve BALB/c mice. Unsupervised clustering of experimental groups based on gene expression profiles. (B) Expression levels of genes associated with neutrophils, PMN-MDSCs, or M1 or M2 macrophages (online supplemental table 3). (C) Volcano plot from the comparison between BM cells stimulated with RPMI or 4T1 TCM. CCRs and CCL are highlighted. (D) CCL3 and CCL4 concentration was evaluated by CBA in the supernatant of BM cells stimulated for 24 hours by the indicated TCMs or recombinant cytokines. The same TCMs incubated for 24 hours without BM cells were used as control. Supernatant from BM cells cultured in RPMI with no stimuli was used as negative control for the cultures with recombinant cytokines. Data derived from two independent experiments. (E) CCL3, CCL4 expression was evaluated by ICS on Lin$^-$population of BALB/c BM cells treated for 4 hours with 4T1-TCM, GM-CSF and interleukin 6, or RPMI. (F) BM from C57BL/6 mice was cultured for 4 hour with MCA203 TCM and evaluated by flow cytometry on HSPC subsets. CCR, chemokine receptors; HSPCs, hematopoietic stem and precursors cells; MDSC, myeloid-derived suppressor cell; MPP, multipotent progenitors; TCM, tumor conditioned media.

performed on BM cells from C57BL/6 mice showed that almost all HSPC subsets secreted these chemokines in response to MCA203 TCM (figure 6F and online supplemental figure 8C). Interestingly, the TCM from the poorly immunogenic tumor CT26 and recombinant IL6 alone did not modulate CCL3 or CCL4 production (figure 6D). It is important to remember that IL6 has a dual and opposite actions on the immune response[30] that are most likely regulated by the signal integration with other factors. For example, GM-CSF and IL6 induced BM cells to differentiate in highly suppressive MDSCs[28] that promoted tumor cell proliferation and did not induce clonotypic T cell proliferation when pulsed with the relevant peptide (online supplemental figure 8D–F). In sharp contrast, BM cells differentiated with only IL6 were not suppressive, did not increase neoplastic cell proliferation, induced clonotypic T cell proliferation when pulsed with the relevant peptide, and contained a large proportion of MHC class II$^+$, CD86$^+$ M1-like macrophages (online supplemental figure 8C–G).

Taken together, these data support the notion that CCR1 and CCR5 regulate the differentiation commitment of myeloid cells through a mechanism that involve the autocrine secretion of CCL3 and CCL4 in response to MDSC inducing factors secreted by neoplastic cells.

CCR1 and CCR5 blockade restrains the generation of human MDSCs

Having shown that CCR1 and CCR5 are required for tumor driven MDSC differentiation in mice, we next evaluated whether a similar pathway regulated tumor induced myelopoiesis in human.

First, we analyzed by flow cytometry the blood and the tumor of patients with recurrent HNSCC or age matched healthy donors to characterize HSPC subsets (online supplemental figure 9). In the blood, we observed the expansion of cells resembling HSC, MPP, CMP, and GMP whereas we found no significant differences in MEP (figure 7A). As observed in mice, at the tumor site MPP-like cells were the most prominent population (figure 7A).

Next, we evaluated whether circulating HSPC-like cells could differentiate into PMN-MDSC-like cells on stimulation with TCM and whether CCR1 and CCR5 antagonists could alter this process. We purified and expanded CD34$^+$ cells from patients with HNSCC and cultured them with TCM with or without B×471 and maraviroc (figure 7B). TCM differentiated HSPC-like cells mostly into CD15$^+$ FSC^{high} CD11b^{low} PMN-MDSCs with only a few CD14$^+$ monocyte-like and CD15$^+$ FSC^{low} CD11b^{high}neutrophils. In sharp contrast, HSPCs cultured with TCM, B×471, and maraviroc differentiated into CD15$^+$ CD11b^{high} FSC^{low} neutrophils with almost no contamination of PMN-MDSCs and monocytes (figure 7B).

Finally, to functionally evaluate the role of CCR1 and CCR5 on human MDSC differentiation, we stimulated UCB-HSPCs with TCMs from human breast cancer cell lines (MDA231, 1833, or 4175) or recombinant cytokines (GM-CSF +G CSF or GM-CSF +IL6) for 4 days with B×471 and maraviroc (figure 7C) or with vehicle as control. In the vehicle group, PMN-MDSCs outnumbered the FSCs^{low} CD11b^{high} neutrophils regardless of the differentiation conditions whereas 'classical' neutrophils outnumbered PMN-MDSCs in the B×471 +maraviroc cultures (figure 7C). When these cells were functionally tested in co-culture experiments with autologous, phytohemagglutinin stimulated CFSE labeled T cells, myeloid cells from the vehicle group induced Foxp3 in most of proliferating T cells[31] whereas those from the B×471 +maraviroc cultures expanded mostly Foxp3$^-$T cells (figure 7D). These results, consistent across all the MDSC inducing conditions tested, indicated that CCR1 and CCR5 mediate tumor-induced MDSC differentiation in humans.

DISCUSSION

Cancer induced 'emergency' hematopoiesis is responsible for the accumulation of protumoral myeloid cells systemically and in the tumor bed, although both protumor PMN-MDSCs and antitumor neutrophils coexist in cancer hosts.[21 32–34] Despite the importance of PMN polarization in cancer host, the molecular pathways that regulate this protumoral process are still not fully understood.

Using an agnostic nanoparticle-based strategy, we first discovered that the silencing of both CCR1 and CCR5 was necessary and sufficient to change the phenotype and function of tumor-infiltrating myeloid cells and restrain tumor progression in all mouse cancer types tested. Importantly, inhibition of both receptors was required to achieve the therapeutic effect, suggesting redundancy, synergy, or integration of the downstream signaling. Phenotypic and functional analysis of the tumor microenvironment pointed us to the presence of classical neutrophils as the main mechanism for the antitumor activity induced by CCR1 and CCR5 silencing. Indeed, we did not observe any changes in the phenotype or number of tumor-infiltrating lymphocytes in mice treated with CCR1 and CCR5 shRNAs but we observed a modification of phenotype and function of PMN-cells, macrophages, and DCs. Additionally, treatment with anti-Ly6G antibody further implicates neutrophil polarization as primarily responsible for the observed antitumor activity. This antibody that depletes PMN but leaves untouched T and NK subsets significantly reduced the therapeutic effects of CCR1 and CCR5 shRNAs but inhibited tumor progression in mice treated with the scrambled shRNAs. A marginal role of T, B and NK cells in the observed antitumor effect is confirmed by our experiment in NSG mice that are devoid to these lymphoid populations. Although these results do not exclude a possible tardive role of the adaptive immunity in mediating cancer control, they do indicate that the relative concentration of PMN-MDSCs and classical neutrophils is key for the observed antitumor effects.

'Classical' neutrophils can exert a strong tumoricidal action directly and in a contact dependent manner by

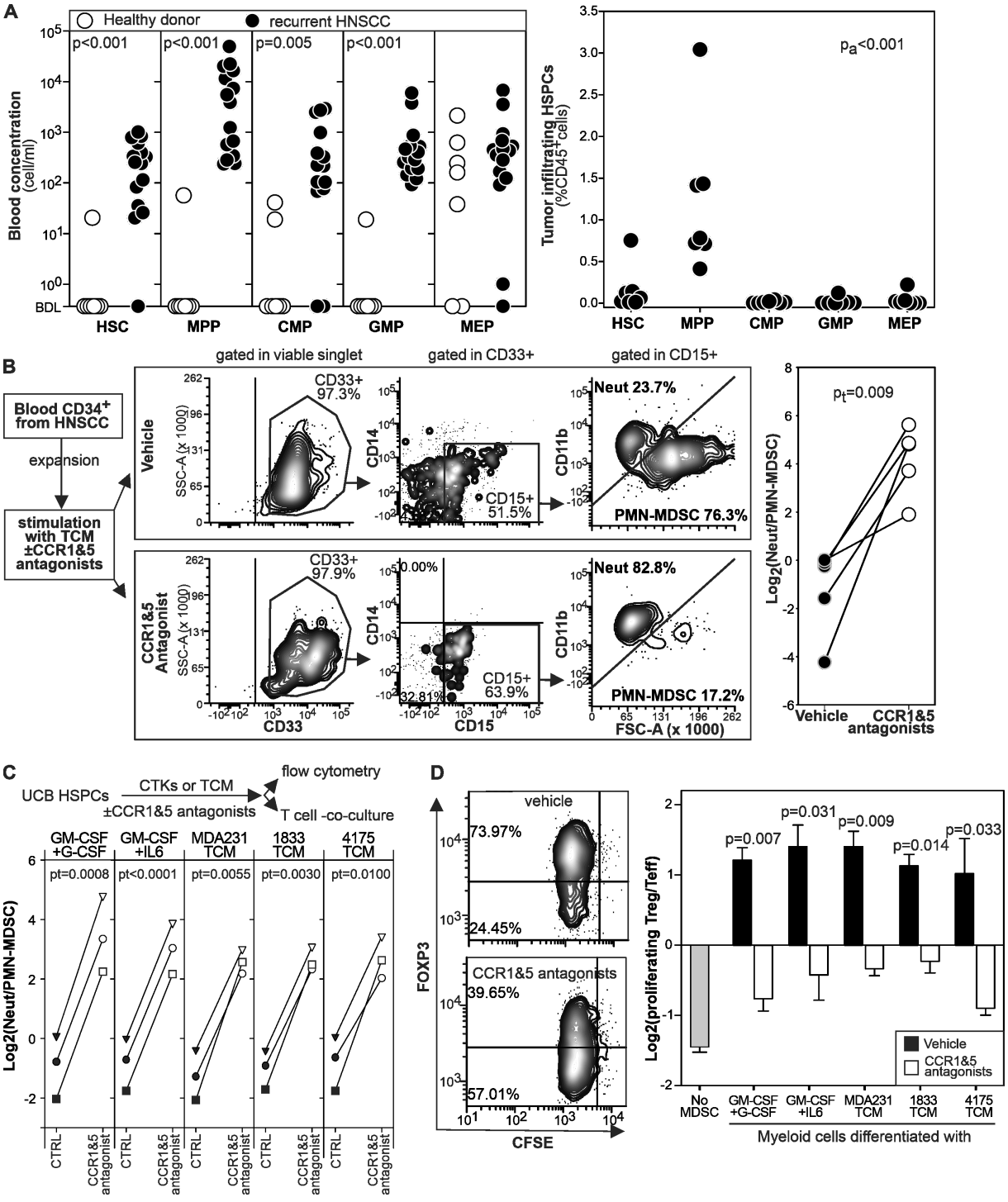

Figure 7 CCR1 and CCR5 antagonists inhibit MDSC differentiation from human HSPCs. (A) The indicated HSPC subsets were enumerated by flow cytometry in the blood and in the tumor of patients with recurrent HNSCC or in age matched healthy controls. (B) Magnetically isolated circulating HSPCs from patients with HNSCC were expanded, stimulated for 4 days with TCM in the presence or in the absence of B×471 and maraviroc, and analyzed by flow cytometry. (C) CD3-depleted, ficolled UCB cells were stimulated for 4 days with cytokines or TCM in the presence or in the absence of maraviroc and B×471. Differentiated cells were then analyzed phenotypically by flow cytometry or in T cell co-culture assays. Neutrophils/PMN-MDSCs ratio of UCB cultures under the indicated conditions are reported. (D) UCB cells differentiated as in (C) were co-cultured with PHA-stimulated autologous, CFSE labeled $CD3^+$cells for 3 days and analyzed by flow cytometry. Log_2 ratio between $Foxp3^+$ 'Treg' and $Foxp3^-$ T effector cells among the $CFSE^{low}$ $CD3^+$ $CD4^+$ cells. Data derived from 2,3 biological replica. CCR, chemokine receptors; HNSCC, head and neck squamous cell carcinoma; HSPCs, hematopoietic stem and precursors cells; MDSC, myeloid-derived suppressor cell; PHA, phytohemagglutinin; PMN, polymorphonuclear; TCM, tumor conditioned media; UCB, umbilical cord blood.

secreting different factors (eg, nitric oxide, hydrogen peroxide, superoxide, lactotransferrin, NETs) and via trogoptosis, or indirectly by promoting adaptive immunity.[32 35–37] In vitro assays using commercially available inhibitors seem to deny the involvement of nitric oxide, lysozyme, superoxide, and NETosis in the tumoricidal action of our 'converted' neutrophils. Although beyond the scope of this manuscript, that focuses on myeloid cell repolarization, the upregulation of lactotransferrin by CCR1 and CCR5 antagonists points to this glycoprotein as putative mediator of neutrophil cytotoxicity.[27]

While most of our data are on neutrophils and PMN-MDSCs, since these are the most abundant populations found in most human and mouse tumors,[38 39] including the models evaluated, we also observed a polarization of macrophages toward an M1-like phenotype in the tumors of mice treated with shRNAs specific for CCR1 and CCR5, and a loss of suppressive activity of Ly6C$^+$m-MDSC differentiated in vitro by tumor derived factors in the presence of CCR1 and CCR5 inhibitors. These effects are not completely surprising since different transcription factors modulated by CCR1 and CCR5,[40–42] such as C/EBPβ or STAT3, play important roles in the polarization of multiple myeloid cell subsets including MDSCs, macrophages, and DCs.[28 43–46] This can also explain why the targeted silencing of CCR1 and CCR5 affects tumor growth across multiple models even when PMN-MDSCs are not the most abundant protumoral myeloid cells like, for example, the MCA203 model.

CCR1 and CCR5 are detectable in most human tumors and are usually associated with leukocyte trafficking.[47] Genetic data, however, indicated a modest chemotactic effect of CCR1 and CCR5 in myeloid cell trafficking and showed the dominant role of CCR2 in this process.[12] Our adoptive cell transfer experiment confirmed these findings and argued against a prominent role of CCR1 and CCR5 in myeloid cell trafficking to the tumor. Instead, we found that the simultaneous inhibition of CCR1 and CCR5 prevents MDSC differentiation driven by tumor derived factors or recombinant cytokines and promotes the generation of neutrophils with a strong antitumor activity. We confirmed these findings in mouse and human not only using HSPCs from naïve mice or from human umbilical cord blood but also using circulating HSPC-like cells from tumor bearing mice and patients with HNSCC. These data indicate that CCR1 and CCR5 play an unexpected role in myeloid cell polarization even if HSPCs-like have been previously sensitized by growing tumors. It is important to note that this is not the first time that CCR1 and CCR5 have been associated with chemotaxis independent functions. For example, both receptors mediate osteoclast differentiation and function and directly enhance cancer cell survival and proliferation, and CCR5 seems to be implicated in MDSC suppression.[48 49]

Our transcriptome analysis further confirmed the involvement of CCR1 and CCR5 in the polarization of myeloid cells, showing that HSPCs differentiated by tumor derived factors in the presence of maraviroc and B×471 shared a signature of classical neutrophils and clustered with CD11b$^+$ cells from the bone marrow of naïve mice, whereas the ones differentiated without antagonists showed an MDSC signature and clustered with tumor-infiltrating myeloid cells.

The transcriptome analysis also revealed that tumor derived factors induced bone marrow cells to transcribe CCL3, CCL4, and other ligands of CCR1 and CCR5. CCL3 and CCL4 are produced by different leukocyte populations and their presence in human malignancies is associated with the presence of protumoral myeloid cells and worse prognosis in mouse models[50 51] and in patients with cancer.[12 52–54]

This autocrine production of CCL3 and CCL4 by HSC, confirmed at the protein level by cytokine beads array and intracellular staining, explained the conundrum that MDSCs can be differentiated in the absence of CCR1 and CCR5 ligands using recombinant cytokines such GM-CSF and IL6 or tumor conditioned media deficient of CCL3 and CCL4. Interestingly, while GM-CSF increases the secretion of both chemokines, IL6, that is co-required for MDSC generation,[28] significantly decreases CCL3 and does not modulate CCL4. IL6 is involved in HSCs expansion and in emergency hematopoiesis[55 56] and has been describe to induce both immune stimulatory and immunosuppressive myeloid cells in different experimental settings.[30] These opposite functions can be explained by the integration of IL6 signaling with the one of other of factors present in the tumor micro-environment and macro-environment. For example, our data confirmed that GM-CSF and IL6 induces highly suppressive MDSC[28] and showed that this combination upregulates CCL3 and CCL4. In sharp contrast, IL6 alone do not differentiate BM cell in MDSC, do not upregulate CCL3 and CCL4, and promote the differentiation of cells capable to stimulate T cell proliferation.

In summary, our data support a model by which cancer-driven protumoral myelopoiesis is regulated by a circuit in which tumor derived factors induce the production of CCL3 and CCL4 and other CCR1 and CCR5 ligands that, by engaging CCR1 and CCR5, autocrinally promote their differentiation into MDSCs.

Contributors Conceptualization: PS; Methodology: SZ, PS, and SB; Software: SB; Investigation: SZ, DW, and PS; Resources: DW and SB; Data Curation: SZ, SB, and PS; Writing—original draft: PS; Writing—review and editing: SZ, SB, DW, and PS; Visualization: SZ and PS; Supervision: PS; Project administration: PS; Funding acquisition: PS, SB, and DW. Guarantor: PS

Funding This study was supported by the DOD-BCRP award W81XWH-13-1-0186 and NIH R21CA263607-01 (to PS), the SCCC translational science award (to PS and DW), the AIRC Special Program Molecular Clinical Oncology '5 per mille', and the Italian Epigenomics Flagship Project (Epigen; to SB) and with facilities supported by the NCI-NIH under Award P30CA240139. The authors thanks Oliver Umland and the DRI flow cytometry core, the SCCC imaging core, and Carla Rodriguez, Ingrid Torrens, and Victoria Kuznetsova for the technical help.

Competing interests PS and SZ are named inventors in the patent WO2016141151A1 filed by the University of Miami, currently licensed to Kerafast, regarding the use of the 4PD nanoparticle.

Patient consent for publication Consent obtained directly from patient(s).

Ethics approval Tumor specimens and blood were collected from patients with head and neck squamous cell carcinoma under a protocol (20200268) approved by the Institutional Review Board (IRB) of the University of Miami. Patients were enrolled after signing the IRB approved written informed consent. Participants gave informed consent to participate in the study before taking part.

Provenance and peer review Not commissioned; externally peer reviewed.

Data availability statement Data are available in a public, open access repository. Data are available upon reasonable request. All data relevant to the study are included in the article or uploaded as supplementary information. Raw data are available at Gene Expression Omnibus under accession number GSE148615.

ORCID iDs
Serena Zilio http://orcid.org/0000-0002-9969-5951
Silvio Bicciato http://orcid.org/0000-0002-1944-7078
Paolo Serafini http://orcid.org/0000-0002-3651-9176

REFERENCES

1 Engblom C, Pfirschke C, Pittet MJ. The role of myeloid cells in cancer therapies. *Nat Rev Cancer* 2016;16:447–62.
2 Noh H, Eomm M, Han A. Usefulness of pretreatment neutrophil to lymphocyte ratio in predicting disease-specific survival in breast cancer patients. *J Breast Cancer* 2013;16:55–9.
3 Reid MD, Basturk O, Thirabanjasak D, *et al*. Tumor-infiltrating neutrophils in pancreatic neoplasia. *Mod Pathol* 2011;24:1612–9.
4 Niitsu N, Khori M, Hayama M, *et al*. Phase I/II study of the rituximab-EPOCT regimen in combination with granulocyte colony-stimulating factor in patients with relapsed or refractory follicular lymphoma including evaluation of its cardiotoxicity using B-type natriuretic peptide and troponin T levels. *Clin Cancer Res* 2005;11:697–702.
5 Albanesi M, Mancardi DA, Jönsson F, *et al*. Neutrophils mediate antibody-induced antitumor effects in mice. *Blood* 2013;122:3160–4.
6 Eruslanov EB, Bhojnagarwala PS, Quatromoni JG, *et al*. Tumor-associated neutrophils stimulate T cell responses in early-stage human lung cancer. *J Clin Invest* 2014;124:5466–80.
7 Caruso RA, Bellocco R, Pagano M, *et al*. Prognostic value of intratumoral neutrophils in advanced gastric carcinoma in a high-risk area in northern Italy. *Mod Pathol* 2002;15:831–7.
8 Hirt C, Eppenberger-Castori S, Sconocchia G, *et al*. Colorectal carcinoma infiltration by myeloperoxidase-expressing neutrophil granulocytes is associated with favorable prognosis. *Oncoimmunology* 2013;2:e25990.
9 Nagarsheth N, Wicha MS, Zou W. Chemokines in the cancer microenvironment and their relevance in cancer immunotherapy. *Nat Rev Immunol* 2017;17:559–72.
10 Flores-Toro JA, Luo D, Gopinath A, *et al*. CCR2 inhibition reduces tumor myeloid cells and unmasks a checkpoint inhibitor effect to slow progression of resistant murine gliomas. *Proc Natl Acad Sci U S A* 2020;117:1129–38.
11 Blattner C, Fleming V, Weber R, *et al*. CCR5^{+} myeloid-derived suppressor cells are enriched and activated in melanoma lesions. *Cancer Res* 2018;78:157–67.
12 Dyer DP, Medina-Ruiz L, Bartolini R, *et al*. Chemokine receptor redundancy and specificity are context dependent. *Immunity* 2019;50:378–89.
13 Yang L, Wang B, Qin J, *et al*. Blockade of CCR5-mediated myeloid derived suppressor cell accumulation enhances anti-PD1 efficacy in gastric cancer. *Immunopharmacol Immunotoxicol* 2018;40:91–7.
14 Hirai H, Fujishita T, Kurimoto K, *et al*. CCR1-mediated accumulation of myeloid cells in the liver microenvironment promoting mouse colon cancer metastasis. *Clin Exp Metastasis* 2014;31:977–89.
15 Shields JD, Kourtis IC, Tomei AA, *et al*. Induction of lymphoidlike stroma and immune escape by tumors that express the chemokine CCL21. *Science* 2010;328:749–52.
16 Weber C, Belge KU, von Hundelshausen P, *et al*. Differential chemokine receptor expression and function in human monocyte subpopulations. *J Leukoc Biol* 2000;67:699–704.
17 Di Marzio P, Dai WW, Franchin G, *et al*. Role of Rho family GTPases in CCR1- and CCR5-induced actin reorganization in macrophages. *Biochem Biophys Res Commun* 2005;331:909–16.
18 Salanga CL, O'Hayre M, Handel T. Modulation of chemokine receptor activity through dimerization and crosstalk. *Cell Mol Life Sci* 2009;66:1370–86.
19 Mantovani A. The chemokine system: redundancy for robust outputs. *Immunol Today* 1999;20:254–7.
20 Zilio S, Vella JL, De la Fuente AC, *et al*. 4PD functionalized dendrimers: a flexible tool for in vivo gene silencing of tumor-educated myeloid cells. *J Immunol* 2017;198:4166–77.
21 Sagiv JY, Michaeli J, Assi S, *et al*. Phenotypic diversity and plasticity in circulating neutrophil subpopulations in cancer. *Cell Rep* 2015;10:562–73.
22 Youn J-I, Kumar V, Collazo M, *et al*. Epigenetic silencing of retinoblastoma gene regulates pathologic differentiation of myeloid cells in cancer. *Nat Immunol* 2013;14:211–20.
23 Maueröder C, Mahajan A, Paulus S, *et al*. Ménage-à-trois: the ratio of bicarbonate to CO_2 and the pH regulate the capacity of neutrophils to form NETs. *Front Immunol* 2016;7:583.
24 Pericle F, Kirken RA, Epling-Burnette PK, *et al*. Direct killing of interleukin-2-transfected tumor cells by human neutrophils. *Int J Cancer* 1996;66:367–73.
25 Attri P, Kaushik NK, Kaushik N, *et al*. Plasma treatment causes structural modifications in lysozyme, and increases cytotoxicity towards cancer cells. *Int J Biol Macromol* 2021;182:1724–36.
26 Furumaya C, Martinez-Sanz P, Bouti P, *et al*. Plasticity in pro- and anti-tumor activity of neutrophils: shifting the balance. *Front Immunol* 2020;11:2100.
27 Cutone A, Rosa L, Ianiro G, *et al*. Lactoferrin's anti-cancer properties: safety, selectivity, and wide range of action. *Biomolecules* 2020;10 doi:10.3390/biom10030456
28 Marigo I, Bosio E, Solito S, *et al*. Tumor-induced tolerance and immune suppression depend on the C/EBPbeta transcription factor. *Immunity* 2010;32:790–802.
29 Bronte V, Chappell DB, Apolloni E, *et al*. Unopposed production of granulocyte-macrophage colony-stimulating factor by tumors inhibits CD8+ T cell responses by dysregulating antigen-presenting cell maturation. *J Immunol* 1999;162:5728–37.
30 Fuster JJ, Walsh K. The good, the bad, and the ugly of interleukin-6 signaling. *EMBO J* 2014;33:1425–7.
31 Zoso A, Mazza EMC, Bicciato S, *et al*. Human fibrocytic myeloid-derived suppressor cells express IDO and promote tolerance via Treg-cell expansion. *Eur J Immunol* 2014;44:3307–19.
32 Zilio S, Serafini P. Neutrophils and granulocytic MDSC: the Janus God of cancer immunotherapy. *Vaccines* 2016;4:31. doi:10.3390/vaccines4030031
33 Eruslanov EB, Singhal S, Albelda SM. Mouse versus human neutrophils in cancer: a major knowledge gap. *Trends Cancer* 2017;3:149–60.
34 Sica A, Guarneri V, Gennari A. Myelopoiesis, metabolism and therapy: a crucial crossroads in cancer progression. *Cell Stress* 2019;3:284–94.
35 Matlung HL, Babes L, Zhao XW, *et al*. Neutrophils kill antibody-opsonized cancer cells by trogoptosis. *Cell Rep* 2018;23:3946–59.
36 Li P, Lu M, Shi J, *et al*. Dual roles of neutrophils in metastatic colonization are governed by the host NK cell status. *Nat Commun* 2020;11:4387.
37 Hedrick CC, Malanchi I. Neutrophils in cancer: heterogeneous and multifaceted. *Nat Rev Immunol* 2021 doi:10.1038/s41577-021-00571-6
38 Cassetta L, Bruderek K, Skrzeczynska-Moncznik J, *et al*. Differential expansion of circulating human MDSC subsets in patients with cancer, infection and inflammation. *J Immunother Cancer* 2020;8:e001223.
39 Youn J-I, Nagaraj S, Collazo M, *et al*. Subsets of myeloid-derived suppressor cells in tumor-bearing mice. *J Immunol* 2008;181:5791–802.
40 Huang R, Wang S, Wang N, *et al*. CCL5 derived from tumor-associated macrophages promotes prostate cancer stem cells and metastasis via activating β-catenin/STAT3 signaling. *Cell Death Dis* 2020;11:234.

41 Lee MMK, Chui RKS, Tam IYS, *et al*. CCR1-mediated STAT3 tyrosine phosphorylation and CXCL8 expression in THP-1 macrophage-like cells involve pertussis toxin-insensitive Galpha(14/16) signaling and IL-6 release. *J Immunol* 2012;189:5266–76.
42 Zhuang Y, Zhao X, Yuan B, *et al*. Blocking the CCL5-CCR5 axis using maraviroc promotes M1 polarization of macrophages cocultured with irradiated hepatoma cells. *J Hepatocell Carcinoma* 2021;8:599–611.
43 Ruffell D, Mourkioti F, Gambardella A, *et al*. A CREB-C/EBPbeta cascade induces M2 macrophage-specific gene expression and promotes muscle injury repair. *Proc Natl Acad Sci U S A* 2009;106:17475–80.
44 Scholz F, Grau M, Menzel L, *et al*. The transcription factor C/EBPbeta orchestrates dendritic cell maturation and functionality under homeostatic and malignant conditions. *Proc Natl Acad Sci U S A* 2020;117:26328–39.
45 Cohen PA, Koski GK, Czerniecki BJ, *et al*. STAT3- and STAT5-dependent pathways competitively regulate the pan-differentiation of CD34pos cells into tumor-competent dendritic cells. *Blood* 2008;112:1832–43.
46 Yin Z, Ma T, Lin Y, *et al*. IL-6/STAT3 pathway intermediates M1/M2 macrophage polarization during the development of hepatocellular carcinoma. *J Cell Biochem* 2018;119:9419–32.
47 Karash A, Mazzoni MR, Gilchrist A. Pharmacological intervention at CCR1 and CCR5 as an approach for cancer: help or hindrance. *Curr Top Med Chem* 2014;14:1553–73.
48 Oba Y, Lee JW, Ehrlich LA, *et al*. MIP-1alpha utilizes both CCR1 and CCR5 to induce osteoclast formation and increase adhesion of myeloma cells to marrow stromal cells. *Exp Hematol* 2005;33:272–8.
49 Ban Y, Mai J, Li X, *et al*. Targeting autocrine CCL5-CCR5 axis reprograms immunosuppressive myeloid cells and reinvigorates antitumor immunity. *Cancer Res* 2017;77:2857–68.
50 Hawila E, Razon H, Wildbaum G, *et al*. CCR5 directs the mobilization of $CD11b^{+}Gr1^{+}Ly6C^{low}$ polymorphonuclear myeloid cells from the bone marrow to the blood to support tumor development. *Cell Rep* 2017;21:2212–22.
51 Zhang Y, Lv D, Kim H-J, *et al*. A novel role of hematopoietic CCL5 in promoting triple-negative mammary tumor progression by regulating generation of myeloid-derived suppressor cells. *Cell Res* 2013;23:394–408.
52 Fang L-Y, Izumi K, Lai K-P, *et al*. Infiltrating macrophages promote prostate tumorigenesis via modulating androgen receptor-mediated CCL4-STAT3 signaling. *Cancer Res* 2013;73:5633–46.
53 Li L, Liu Y-D, Zhan Y-T, *et al*. High levels of CCL2 or CCL4 in the tumor microenvironment predict unfavorable survival in lung adenocarcinoma. *Thorac Cancer* 2018;9:775–84.
54 Lien M-Y, Tsai H-C, Chang A-C, *et al*. Chemokine CCL4 induces vascular endothelial growth factor C expression and lymphangiogenesis by miR-195-3p in oral squamous cell carcinoma. *Front Immunol* 2018;9:412.
55 Tie R, Li H, Cai S, *et al*. Interleukin-6 signaling regulates hematopoietic stem cell emergence. *Exp Mol Med* 2019;51:1–12.
56 Suda T, Yamaguchi Y, Suda J, *et al*. Effect of interleukin 6 (IL-6) on the differentiation and proliferation of murine and human hemopoietic progenitors. *Exp Hematol* 1988;16:891–5.

Supplemental methods

Flow Cytometry

Flow cytometry was performed on a daily-calibrated flow cytometer, using titrated and validated antibody controls, vital dye, automatic compensation using single-color staining, and FMO or isotype antibodies as negative controls. Antibodies used are indicated in supplemental table 2. Purified CCL4 antibody were conjugated with AlexaFluor™488 Antibody Labeling Kit and used with the BD Cytofix/Cytoperm™Plus kit following manufactured instructions. Mouse and human FoxP3 intracellular staining were performed using eBioscience™ Foxp3/Staining Buffer. Dead cells were excluded by the analysis by using LIVE⁄DEAD® Stain. Samples were read on a LSR2 (BD Bioscience) equipped with 405nm, 488nm, 532nm, and 635nm lasers or Cytoflex (Beckman Coulter) equipped with 405nm, 488nm, 561nm, and 638nm lasers. Sortings were performed on the MoFlo Astrios cell sorter (Beckman Coulter). Data were analyzed using FCSexpress-plus vs7(Denovo-Software).

Image Cytometry

4 µm thick sections from FFPE tumors underwent deparaffination and antigen retrieval with TRIS-EDTA (pH=9). Section were then incubated with Image-iT™FX-Signal-Enhancer (Invitrogen) (30' @RT), with blocking solution (1h @RT, PBS 1x/Triton-x100 0,02%/FBS 10%) and with the purified rabbit monoclonal-anti-Rb primary antibody (Abcam, clone:EPR17512) and purified rat monoclonal anti-mouse anti-LAMP-2 (CD107b) antibody (BioLegend, clone M3/84) (ON @ 4ºC). Sections were washed and incubated 2hs @RT with donkey anti-Rabbit AF647 AffiniPure (Jackson Labs) and donkey anti-Rat AF555 (Invitrogen), section were washed and then incubated 1.5 hs with AF488-conjugated rat anti-mouse Ly6G (BioLegend, clone:1A8). Stained slides were scanned at 20X with the VS120 microscope (Olympus) using DAPI, FITC and TRITC and Cy5 cubes. Tiff files were processed with cellprofiler (www.cellprofiler.com, Supplemental Fig.3) and fed into FCSexpress-plus vs7(Denovo software).

Quantitative RT-PCR

Trizol extracted RNA was retrotranscribed with the High-Capacity-cDNA-Reverse-Transcription Kit and amplified using TaqMan probes and the TaqMan-Fast-Universal-PCR-Master-Mix kit on the StepOnePlus™thermocycler.

Cytokine Beads Array

CCL2, CCL3, CCL4, and CCL5 were quantified using a custom MILLIPLEX® Multiplex Assays (Millipore-Sigma) following manufacturer instruction.

Cell isolation

Human CD3$^+$ and CD3$^-$ cells from UCB were isolated using the Pan T Cell Isolation Kit, human (Miltenyi Biotec). *Mouse CD11b$^+$cells* have been magnetically isolated from tumor and/or spleen of tumor bearing mice using the CD11b Microbeads, human and mouse kit (Miltenyi Biotec) according to manufacturer instruction.

Mouse tumor infiltrating HSPCs have been isolated from a pool of fourteen 4T1 tumors. Tumor single cell suspensions were depleted of Lineage positive cells using the Direct Lineage Cell Depletion Kit, mouse (Miltenyi Biotec) following manufacturer instruction, stained with Anti-Mouse Lineage cocktail and anti-CD45 (Biolegend), and sorted by FACS as viable CD45$^+$/Lin$^-$ cells.

Human CD34$^+$cells from the blood of HNSCC patients were isolated from PBMCs of patients with recurrent HNSCC using the diamond CD34$^+$isolation kit (Miltenyi Biotec) following manufacturer's instructions.

MDSC differentiation and Functional assays

MDSC differentiation. 6x10^5 BM cells were cultured in 30% TCM or complete media with either rmGM-CSF and rmIL6, rmGM-CSF and rmG-CSF, or rmIL6 alone (40 ng/mL each) in low adherence 24 well plate for 4 days. Maraviroc (10 µM) and/or Bx471 (5 µM) were added on day 0 and 3 when indicated.

Mouse MDSCs differentiation from sorted tumor infiltrating HSPCs. HSPCs have been differentiated into MDSCs using the 4T1 TCM as previously above, in presence of CCR1 and CCR5 inhibitors or relative vehicle.

Human-MDSC differentiation from UCB. Ficolled purified, RBC lysed UCB were magnetically depleted by CD3$^+$cells and 2×10^6 cells/well cultured for 4 days in 24-well ultra-low attachment plates (Corning) in RPMI 15% FBS media with rhuGM-CSF and rhuG-CSF, rhuGM-CSF and rhuIL6, or with tumor conditioned media from MDA-MB231, 1833 or 4175.

Expansion of circulating HSPCs from HNSCC and MDSC differentiation. CD34$^+$cells, purified from PBMCs of patients with recurrent HNSCC using the Miltenyi diamond CD34$^+$isolation kit following manufacturer's instructions, (50,000 cells/mL) were expanded in U-bottom 96 well plate in 200 µL of StemSpan™ SFEM media (Stemcells technology) supplemented with stem cell factor (100 ng/mL), FLT3 (100 ng/mL), thrombopoietin (100 ng/mL) IL3 (20 ng/mL) for 1-2 weeks and maintained at a concentration of ~2.5x10^5/mL by dilution with cytokine containing expansion media every 3-4 days. Cells were then washed twice and 2.5x10^5 cells plated in 1 mL of TCM or complete media in 24 well plate.

Mouse-MDSCs suppressive assay. 10^5 CFSE labeled splenocytes from Cl4 mice or OT1 were stimulated with

the relevant peptide (1 μM) in the presence of 10^6 syngeneic splenocytes and syngeneic CD11b$^+$cells for 3 days in 96 well flat bottom plates. Proliferation was evaluated by flow cytometry on the viable CD3$^+$CD8$^+$population.

Human-MDSCs suppressive assay. 10^5 magnetically purified, CFSE labeled, CD3$^+$T cells from UCB were stimulated by PHA (6%) in AIM-V media (Gibco) for 3 days in 96-well U-bottom plates in the presence or absence of 5×10^4 UCB-derived autologous MDSC cells. HEK-293 cells were used as non-suppressive control.

Tumor-Myeloid cell co-culture assay. Magnetically isolated CD11b$^+$cells (purity >90% by flow cytometry) or FACS sorted Ly6G or Ly6C cells were cultured at different ratio with $0.2x10^5$ 4T1-luciferase cells, in complete medium for 18h at 37°C. 4T1-luciferase cells were enumerated using the Li-COR system by luciferase assay after a 5' incubation with luciferin at 37ºC using a freshly diluted known number of 4T1-luciferase cells as standard curve. Inhibitors targeting the main neutrophil tumoricidal pathway were chosen through a literature search, used at optimal reported concentration, and added to the cultures.

Analysis of microarray gene expression data

Twenty-four hours after culture with RPMI, 4T1 TCM with Bx471 and Maraviroc, or 4T1 TCM with vehicle, BM cells were washed with PBS and RNA extracted by Trizol (Invitrogen) and cleaned with RNeasy columns (Qiagen). For each chip, 2.5 μg of total RNA was amplified to biotinylated complementary RNA (cRNA) as described in the Affymetrix GeneChip® Expression Analysis Technical Manual. Pre-hybridization quality controls were performed with the Agilent 2100 bioanalyzer (Agilent Technologies). RNA from 3 biological replicates was then hybridized on Affymetrix MG-U74Av2 arrays. Microarray probe fluorescence signals were converted to $\log_2$ expression values using the Robust Multiarray Average procedure of the *affy* Bioconductor package in R. Briefly, fluorescence intensities were background-adjusted and normalized using quantile normalization, and expression values were calculated using median polish summarization and a custom chip definition file for the Mouse Gene 2.0 ST array based on Entrez genes (mogene20st_Mm_ENTREZG version 21.0.0). Raw data are available at Gene Expression Omnibus under accession number GSE148615.

To identify differentially expressed genes, we compared the expression levels of BM cells cultured in 4T1-TCM and in complete media (RPMI) using the Significance Analysis of Microarray (SAM) algorithm coded in the *samr* R package. [1] In SAM, we estimated the percentage of false positive predictions (i.e. False Discovery Rate, FDR) with 100 permutations and selected those gene IDs with FDR ≤ 5% and absolute fold change larger than a selected threshold (e.g. ≥ 2). The volcano plot, showing the most significantly differentially expressed genes in

the comparison of BM CD11b$^+$cells from 4T1-TCM and complete media (RPMI), was generated using the *ggplot* function of the *ggplot2* R package. P-values were derived from SAM q-values using the function *samr.pvalues.from.perms* of the *samr* R package.

The gene expression levels of CD11b$^+$cells from BM cells cultured with RPMI, 4T1-TCM with vehicle and 4T1-TCM with Bx471 and Maraviroc have been merged with publicly available gene expression data of CD11b$^+$cells. Specifically, gene expression data of CD11b$^+$cells infiltrating 4T1 tumors (MDSC; GSM545536, GSM545537, and GSM545538) and of CD11b$^+$cells isolated from the BM (BM CD11b$^+$; GSM545545, GSM545546, and GSM545547) and from the spleen (splenic CD11b$^+$; GSM545524, GSM545525, and GSM545526) of naïve BALB/c mice were obtained from GSE21927. Raw .CEL files were converted to $\log_2$ expression values using the Robust Multiarray Average procedure of the *affy* Bioconductor package in R a custom chip definition file for the Affymetrix Mouse Genome 430 2.0 arrays based on Entrez genes (Mouse4302_Mm_ENTREZG version 21.0.0). Transcriptional data of the samples hybridized on the different microarray platforms have been merged matching the 17,677 common Entrez Gene IDs of the two custom CDFs. A direct merging of raw fluorescence signals (i.e., of CEL files), although desirable for an optimal removal of batch effects, was unfeasible due to the different probe sequences synthesized on the two types of microarrays. Consequently, batch effects have been removed applying the *ComBat* function of the *sva* Bioconductor package to the merged matrix. *ComBat* was used with default parameters.

Unsupervised and supervised clustering were performed using the function *hclust* of R stats package with Pearson correlation as distance metric and average agglomeration method. Before unsupervised clustering, to reduce the effect of noise from non-varying genes, we removed those Entrez Gene IDs with a coefficient of variation smaller than the median of the coefficients of variation in the entire dataset. Gene expression heatmaps have been generated using the function *heatmap.2* of R gplots package after row-wise standardization of the expression values.

Over-representation analysis was performed using Gene Set Enrichment Analysis and gene sets derived from the Hallmark and BioCarta pathway collections of the Molecular Signatures Database (MSigDB; https://www.gsea-msigdb.org/gsea/msigdb). The GSEA software (http://www.broadinstitute.org/gsea/index.jsp) was applied on log2 expression data of BM cells cultured in 4T1-TCM without CCR1 and CCR5 antagonists (4T1-TCM vehicle), in 4T1-TCM supplemented with CCR1 and CCR5 antagonists (4T1-TCM+antagonists), and

in complete media (RPMI). Gene sets were considered significantly enriched at FDR <5% when using Signal2Noise as metric and 1,000 permutations of gene sets. Except for the over-representation analysis, all data analyses were performed in R version 3.5.1.

Supplemental table 1: material and reagents

REAGENT or RESOURCE	SOURCE	IDENTIFIER
Antibodies		
Rat anti-Mouse CCL3	ThermoFisher Scientific	Cat# 12-7532-82, RRID:AB_2572662
Goat anti-Mouse CCL4	Abcam	Cat# ab10386, RRID:AB_2071053
Rat anti-Mouse CCR1	BioLegend	Cat# 152506, RRID: AB_2687211
Hamster anti-Mouse CCR5	BioLegend	Cat# FAB1802A, RRID: AB_357091
Hamster anti-Mouse CCR5	BioLegend	Cat# 107006, RRID: AB_313301
Rat anti-Mouse CD11b	BD Biosciences	Cat# 562950, RRID: AB_2737913
Rat anti-Mouse CD11b	BD Biosciences	Cat# 550993, RRID: AB_394002
Rat anti-Mouse CD11b	BD Biosciences	Cat# 563168, RRID:AB_2716860
Hamster Anti-Mouse CD11c	BD Biosciences	Cat# 558079, RRID: AB_647251
Rat anti-Mouse CD150	BioLegend	Cat# 115918, RRID:AB_2239178
Rat anti-Mouse CD150	BioLegend	Cat# 115926, RRID:AB_2562190
Rat anti-Mouse CD117	BD Biosciences	Cat# 553356, RRID:AB_398536
Rat anti-Mouse CD117	BD Biosciences	Cat# 563399, RRID:AB_2738183
Rat anti-Mouse CD16/CD32	BD Biosciences	Cat# 553142 RRID: AB_394657
Rat anti-Mouse CD16/32	BioLegend	Cat# 101333, RRID:AB_2563692
Rat anti-Mouse CD206	BioLegend	Cat# 141723, RRID AB_2562445
Rat anti-Mouse CD206	BioLegend	Cat#141729 RRID: AB_2565823
Rat anti-Mouse CD24	BioLegend	Cat# 101808, RRID: AB_312841
Rat anti-Mouse CD3	ThermoFisher Scientific	Cat# 46-0032-82 RRID: AB_1834427
Hamster anti-Mouse CD34	BioLegend	Cat# 128610, RRID:AB_2074601
Rat anti-Mouse CD4	BD Biosciences	Cat# 553049 RRID: AB_394585
Rat anti-Mouse CD45	BioLegend	Cat# 103154, RRID:AB_2572116
Rat anti-Mouse CD45	BD Biosciences	Cat# 557659, RRID:AB_396774
Hamster Anti-Mouse CD48	BioLegend	Cat# 103422, RRID:AB_2075051
Rat anti-Mouse CD8	BD Biosciences	Cat# 553033, RRID:AB_394571
Rat anti-Mouse CD8	BD Biosciences	Cat# 563046, RRID:AB_2737972
Rat anti-Mouse F4/80	AbD Serotec	Cat# MCA497F, RRID: AB_322047
Rat anti-Mouse FoxP3	ThermoFisher Scientific	Cat# 17-5773-80, RRID: AB_469456
Rat anti-Mouse Ly6G	BD Biosciences	Cat# 560600, RRID:AB_1727561
Rat anti-Mouse Ly6G	BD Biosciences	Cat# 560601, RRID:AB_1727562
Rat anti-Mouse Ly6C	BD Biosciences	Cat# 560594, RRID:AB_1727559
Rat anti-Mouse Ly6C	BD Biosciences	Cat# 553104, RRID:AB_394628
Rat anti-Mouse I-A/I-E	BioLegend	Cat# 107606, RRID: AB_313321
Rat anti-Mouse I-A/I-E	BD Biosciences	Cat# 557000, RRID: AB_396546
Anti-Mouse Lineage cocktail	BioLegend	Cat# 133310, RRID:AB_11150779
Anti-Mouse Lineage cocktail	BioLegend	Cat# 133302, RRID:AB_10697030,
Rat anti-Mouse Sca-1	BioLegend	Cat# 108114, RRID:AB_493596
Mouse anti-Human CD11b	BD Biosciences	Cat# 562723, RRID:AB_2737746
Mouse anti-Human CD123	BioLegend	Cat# 306016, RRID:AB_2264693
Mouse anti-Human CD14	BD Biosciences	Cat# 557831, RRID:AB_396889
Mouse anti-Human CD15	BD Biosciences	Cat# 563142, RRID:AB_2738026
Mouse anti-Human CD3	BD Biosciences	Cat# 552851, RRID:AB_394492
Mouse anti-Human CD33	BD Biosciences	Cat# 555626, RRID:AB_395992
Mouse anti-Human CD34	BioLegend	Cat# 343616, RRID:AB_2629726
Mouse anti-Human CD38	BioLegend	Cat# 303506, RRID:AB_314358
Mouse anti-Human CD4	BD Biosciences	Cat# 558116, RRID:AB_397037
Mouse anti-Human CD45	BioLegend	Cat# 304036, RRID:AB_2561940
Mouse anti-Human CD45R	BioLegend	Cat# 103227, RRID:AB_492876
Mouse anti-Human CD8	BD Biosciences	Cat# 557746, RRID:AB_396852
Mouse anti-Human CD90	BioLegend	Cat# 328114, RRID:AB_893431
Mouse anti-Human FoxP3	ThermoFisher Scientific	Cat# 17-4777-42, RRID:AB_10804651
Anti-Human Lineage cocktail	BioLegend	Cat# 348801, RRID:AB_10612570
Rat anti-Mouse Ly6G	BioLegend	Cat#127626, RRID: AB_2561340
Rat Anti-momuse CD107b (LAMP2)	BioLegend	Cat# 108502, RRID: AB_313383
Rabbit anti-Mouse Rb	Abcam	Cat# ab181616, RRID: N/A
AF488 F(ab')$_2$ Donkey Anti-Rabbit IgG	Jackson ImmunoResearch	Cat# 711-546-152, RRID:AB_2340619

Biological Samples			
UCB		New York Blood Center, Long Island City, NY, USA	N/A
Blood from HNSCC patients		University of Miami Hospital, Miami, FL, USA	ClinicalTrials.gov Identifier: NCT02544880
Chemicals, Peptides, Recombinant Proteins, and cell culture media			
DAPI (4′,6-diamidino-2-phenylindole)		ThermoFisher Scientific	Cat# D1306, RRID:AB_2629482
eBioscience™ CFSE		ThermoFisher Scientific	Cat# 65-0850-84
CellTrace™ Far Red Cell Proliferation Kit		ThermoFisher Scientific	Cat# C34564
LIVE/DEAD™ Fixable Near-IR Dead Cell Stain Kit		ThermoFisher Scientific	Cat# L34976
LIVE/DEAD™ Fixable Yellow Dead Cell Stain Kit		ThermoFisher Scientific	Cat# L34968
Zombie Violet™ Fixable Viability Kit		BioLegend	Cat# 423114
VivoGlo™ Luciferin, In Vivo Grade		Promega	Cat# P1042
Collagenase IV from Clostridium histolyticum		Millipore Sigma	Cat# C5138-500MG
Animal-Free Recombinant Human IL-6		PeproTech	Cat# AF-200-06
Animal-Free Recombinant Murine IL-6		PeproTech	Cat# AF-216-16
Animal-Free Recombinant Human GM-CSF		PeproTech	Cat# AF-300-03
Animal-Free Recombinant Murine GM-CSF		PeproTech	Cat# AF-315-03
Animal-Free Recombinant Human G-CSF		PeproTech	Cat# AF-300-23
Animal-Free Recombinant Mouse G-CSF		PeproTech	Cat# AF-250-05
Animal-Free Human Flt3 Ligand		PeproTech	Cat# AF-HHSC3
Animal-Free Human SCF		PeproTech	Cat# AF-HHSC3
Animal-Free Human TPO		PeproTech	Cat# AF-HHSC3
Animal-Free Human IL-3		PeproTech	Cat# AF-HHSC3
Animal-Free Human Hematopoietic Stem Cell Expansion Cytokine Package (IL-3)		PeproTech	Cat# AF-HHSC3
Influenza HA(518-526)		AnaSpec	Cat# AS-21158
OVA (257-264)		AnaSpec	Cat# AS-60193-1
PHA Reagent Grade		ThermoFisher Scientific	Cat# R30852701
Maraviroc		Millipore Sigma	PZ0002-5MG, CAS Number 376348-65-1
Bx471		Millipore Sigma	SML0020, CAS Number: 217645-70-0
4PD in vivo MDSC/ Transfection Kit		Kerafast	Cat# EMI007
Cardiolipin sodium salt from bovine heart		Millipore Sigma	Cat# C0563
StemSpan SFEM		Stem Cell Technologies	Cat # 09650
RPMI 1640 Medium, GlutaMAX™ Supplement		ThermoFisher Scientific	Cat# 61870036
Keratinocyte SFM (1X)		ThermoFisher Scientific	Cat# 17005042
AIM-V media		ThermoFisher Scientific	Cat# 12055091
Image-iT™FX-Signal-Enhancer		ThermoFisher Scientific	Cat# I36933
TRIzol™ Reagent		ThermoFisher Scientific	Cat# 15596018
Histopaque®-1077		Millipore Sigma	Cat# 10711
Complete media	RPMI1640	ThermoFisher Scientific	Cat# A1049101
	Heat inactivated FBS 10%	ThermoFisher Scientific	Cat# 16000044
	HEPES 10mM	ThermoFisher Scientific	Cat# 15630080
	Penicillin-Streptomycin (50U/ml)	ThermoFisher Scientific	Cat#15070063
	L-Glutamine (2 mM)	ThermoFisher Scientific	Cat# 25030081

Critical Commercial Assays		
CD11b MicroBeads, human and mouse	Miltenyi Biotec	Cat# 130-049-601
Pan T Cell Isolation Kit, human	Miltenyi Biotec	Cat# 130-096-535
Diamond CD34 Isolation Kit, human	Miltenyi Biotec	Cat# 130-094-531
Direct Lineage Cell Depletion Kit, mouse	Miltenyi Biotec	Cat# 130-110-470
MILLIPLEX MAP Mouse Cytokine/Chemokine Magnetic Bead Panel - Immunology Multiplex Assay	Millipore Sigma	Cat# MCYTOMAG-70K (custom)
Fixation/Permeabilization Solution Kit with BD GolgiPlug™	BD Biosciences	Cat# 555028
eBioscience™ Foxp3/Staining Buffer Set	ThemoFisher Scientific	Cat# 00-5521-00
High-Capacity cDNA Reverse Transcription Kit	Applied Biosystems	Cat# 4368813
TaqMan-Fast Universal PCR Master Mix (2X), no AmpErase™ UNG" kit	Applied Biosystems	Cat# 4367846
mCCR1 Mm00438260_s1	Applied Biosystems	Cat# 4331182
mCCR2 Mm04207877_m1	Applied Biosystems	Cat# 4331182
mCCR5 Mm01963251_s1	Applied Biosystems	Cat# 4331182
mCCR7 Mm01301785_m1	Applied Biosystems	Cat# 4331182
Eukaryotic 18S rRNA Hs99999901_s1	Applied Biosystems	Cat# 4331182
AlexaFluor488 Antibody Labeling Kit	ThermoFisher Scientific	Cat# A20181
Affymetrix Mouse Gene ST 2.0 Array	Applied Biosystems	Cat# 902118
Deposited Data		
GeneChip raw data		GSE148615
gene expression data of CD11b$^+$cells infiltrating 4T1 tumors		GSM545536, GSM545537, GSM545538
gene expression data of CD11b$^+$cells isolated from the BM		GSM545545, GSM545546, GSM545547
gene expression data of CD11b$^+$cells from the spleen of Naïve BALB/c		GSM545524, GSM545525, GSM545526
Experimental Models: Cell Lines		
4T1HAThy1.1luciferase	provided by I. Borrello (Johns Hopkins University, Baltimore, MD, USA) [2]	N/A
4T1	ATCC® [3]	Cat# CRL-2539, RRID:CVCL_0125RL-2539™
CT26	ATCC® [4]	Cat# CRL-2638, RRID:CVCL_7256
TS/A	provided by V. Bronte (University of Verona, Verona, Italy)[5]	RRID:CVCL_F736
MCA203	provided by V. Bronte (University of Verona, Verona, Italy) [6]	N/A
B16Lu8	provided by V. Bronte (University of Verona, Verona, Italy) [7]	N/A
DA3	provided by D. Lopez (University of Miami, Miami, FL, USA) [8]	RRID:CVCL_5419
B4B8	provided by G. Thomas (University of Miami, Miami, FL, USA) [9]	RRID:CVCL_0B35
MDA-MB231	ATCC® [10]	Cat# HTB-26, RRID:CVCL_0062
MDA-BoM-1833	provided by M. Lippman (University of Miami, Miami, FL, USA) [10]	RRID:CVCL_DP48
MDA231-LM2-4175	provided by M. Lippman (University of Miami, Miami, FL, USA) [10]	RRID:CVCL_5998

Experimental Models: Organisms/Strains		
BALB/cJ	The Jackson Laboratory	IMSR Cat# JAX:000651, RRID:IMSR_JAX:000651
C57BL/6J	The Jackson Laboratory	IMSR Cat# JAX:000664, RRID:IMSR_JAX:000664
CCR5KO mice B6.129P2-Ccr5<tm1Kuz>/J,	The Jackson Laboratory	IMSR Cat# JAX:005427, RRID:IMSR_JAX:005427
CBy.PL(B6)-*Thy1*^{a}/ScrJ	The Jackson Laboratory	IMSR Cat# JAX:005443, RRID:IMSR_JAX:005443
Cl.4 mice (Tg(TcraCl4,TcrbCl4)1 Shrm/ShrmJ) BALB/c	Gift from E. Sotomayor	IMSR Cat# JAX:005686, RRID:IMSR_JAX:005686
OT1 C57BL/6-Tg(TcraTcrb)1100Mjb/J	The Jackson Laboratory	IMSR Cat# JAX:003831, RRID:IMSR_JAX:003831
CCR1KO B6.129S-*Ccr1*^{tm1Gao}/AdlJ	Provided by P. Murphy (NIH)	IMSR Cat# JAX:032932, RRID:IMSR_JAX:032932

Oligonucleotides		
name	**Reference**	**sequence**
mCCR1-m3xRT3	[11] Eurofins genomics	5′TTTGACCTTCTTCTCACTGGGTCTTC3′
mCCR1-m3xs300	[11] Eurofins genomics	5′GCTGTCTCTGATCTGGTCTTCCTT3′
CCR1-m3xs600	[11] Eurofins genomics	5′GAGTTCACTCACCGTACCTGTAGC3′
Neo Cassette ANeo	[11] Eurofins genomics	5′TGGGTGGAGAGGCTTTTTGCTTCCTCTTGC3′
mCCR5-5oIMR0700	https://www.jax.org/Protocol?stockNumber=002782&protocolID=22436	5′CAGGCAACAGAGACTCTTGG3′
Primer for mCCR5 oIMR0701	https://www.jax.org/Protocol?stockNumber=002782&protocolID=22436	5′-TCATGTTCTCCTGTGGATCG-3′
Primer for Neo Cassette oIMR6916	https://www.jax.org/Protocol?stockNumber=002782&protocolID=22436	5′-CTTGGGTGGAGAGGCTATTC-3′
Primer for Neo Cassette oIMR6917	https://www.jax.org/Protocol?stockNumber=002782&protocolID=22436	5′-AGGTGAGATGACAGGAGATC-3′
mCCR1shRNA	[12] Oligofactory	GGfUfCfUAAGAAGAGAAfUGAGfUfUfCAAGAGAfCfUfCAfUfUfCfUfCfUfUfCfUfUAGAfCfCfUfUfUfUfU
mCCR2shRNA	[13] Oligofactory	GfCfUAAAfCGfUfCfUfCfUGfCAAGfUfUfCAAGAGAfUGfCfUAAAfCGfUfCfUfCfUGfCAAAfUfUfUfUfU
mCCR5 shRNA	[14] Oligofactory	GGfUfUfCfUGAGAfUfCfUGGfUAAAGAfUfUfCAAGAGAfUfCfUfUfUfUAfCfCAGAfUfCfUfCAGAAfUfUfUfUfU
mCCR7 shRNA	[15] Oligofactory	GGfCfCfUfCAfUfUAfUfCAfUfCfCGfUAfCfCfUfUfCAAGAGAGGfUAfCGGAfUGAfUAAfUGAGGfUfUfUfUfU
Scrambled-mCCR1 shRNA	Oligofactory	GGAfUAAGAfUGfCGfUAGAAGAfUfUfCAAGAGAfUfCfUfUfCfUAfCGfCAfUfCfUfUAfUfCfCfUfUfUfUfU
Scrambled-mCCR2-shRNA	Oligofactory	GAGfCGfUfCGfCAAfUAfCAfUfCfUGfUfUfCAAGAGAGAfUGfUAfUfUGfCGAfCGfCfUfUfUfUfUfUfU
Scrambled-mCCR5-shRNA	Oligofactory	GGAGfUAfUGAGAfUAfUAfCGfUfCfUGfUfUfCAAGAGAfCAGAfCGfUAfUAfUfCfUfCAfUAfCfUfUfUfUfUfU
Scrambled-mCCR7-shRNA	Oligofactory	GGAfUfCfUfCfCAfUfCGfCfCfUAfUfCfCfUAfUfUfCAAGAGAfUAGGAfUAGGfCGAfUGGAGAfUfUfUfUfUfU

Software and Algorithms		
Sigmaplot 12.5	Systat software	https://systatsoftware.com/products/sigmaplot/
FCS express 7 plus	Denovo software	https://denovosoftware.com/
Cell profiler	[16]	www.cellprofiler.com
Total Image slicer		https://www.coolutils.com/
ImageJ	[17]	https://fiji.sc/
OlyVIA Ver.2.9.1 (Build 13771)	Olympus	https://www.olympus-lifescience.com/en/support/downloads/#!dlOpen=%23detail847252030
R Package: Robust Multiarray Average procedure of the *affy* Bioconductor	[18]	
Samr R package (Significance Analysis of Microarray (SAM) algorithm)	[1]	
Molecular Signatures Database (MSigDB)		https://www.gsea-msigdb.org/gsea/msigdb
GSEA software		http://www.broadinstitute.org/gsea/index.jsp

Table S3 genes associated with PMN-MDSC, neutrophils, M1 macrophages, or M2 macrophages

Gene	Associated with	Reference	Gene	Associated with	Reference
Vegfa	PMN-MDSC	[19]	CCR7	M1	[20]
Tnf	PMN-MDSC	[21]	Gpr18	M1	[20]
Mpo	PMN-MDSC	[22]	Myc	M2	[20]
MMP9	PMN-MDSC	[21]	Retnla	M2	[20]
IL6	PMN-MDSC	[23]	Mrc1	M2	[20]
CXCL2	PMN-MDSC	[21]	Egr2	M2	[20]
CD274	PMN-MDSC	[24]	Chil3	M2	[20]
CXCL10	PMN-MDSC	[21]	CD83	M2	[20]
CXCL1	PMN-MDSC	[21]	Adgre1	macrophage	[25]
CD244	PMN-MDSC	[21]	Flot2	neutrophils	[26]
Cebpb	PMN-MDSC	[27]	CXCL12	neutrophils	[27]
CCL3	PMN-MDSC	[21]	Tuba4a	neutrophils	[26]
CCL2	PMN-MDSC	[21]	CXCR1	neutrophils	[27]
CCL17	PMN-MDSC	[21]	Elane	neutrophils	[28]
Arg1	PMN-MDSC	[19]	Foxo4	neutrophils	[26]
Ptges2	PMN-MDSC	[27]	S100a11-ps	neutrophils	[26]
Tgfb1	PMN-MDSC	[27]	Lamp2	neutrophils	[19]
Ddit3	PMN-MDSC	[27]	Pf4	neutrophils	[27]
Csf1r	PMN-MDSC	[27]	Ifng	neutrophils	[21]
CXCL14	PMN-MDSC	[23]	Icam1	neutrophils	[21]
Fpr2	M1	[20]	CXCL13	neutrophils	[23]
Nos2	M1	[25]	CCL6	neutrophils	[23]
IL12b	M1	[20]	CXCR2	neutrophils	[27]
CXCL9	M1	[20]	Itgb2l	neutrophils	[21]
CD38	M1	[20]	Slc4a1	neutrophils	[21]

SUPPLEMENTAL FIGURES

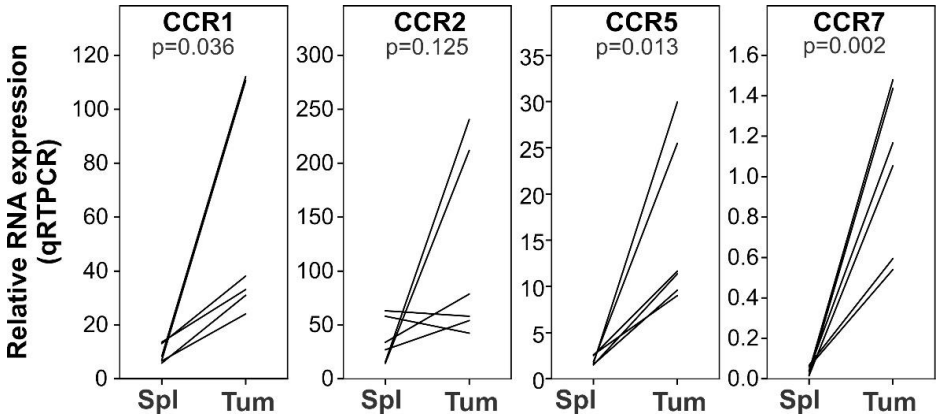

Supplemental figure 1: CCR1, CCR5, and CCR7 are upregulated in the tumor microenvironment. Expression of the indicated chemokine receptors was evaluated on $CD11b^{+}$cells magnetically isolated from the tumor or the spleen of 4T1 bearing mice.

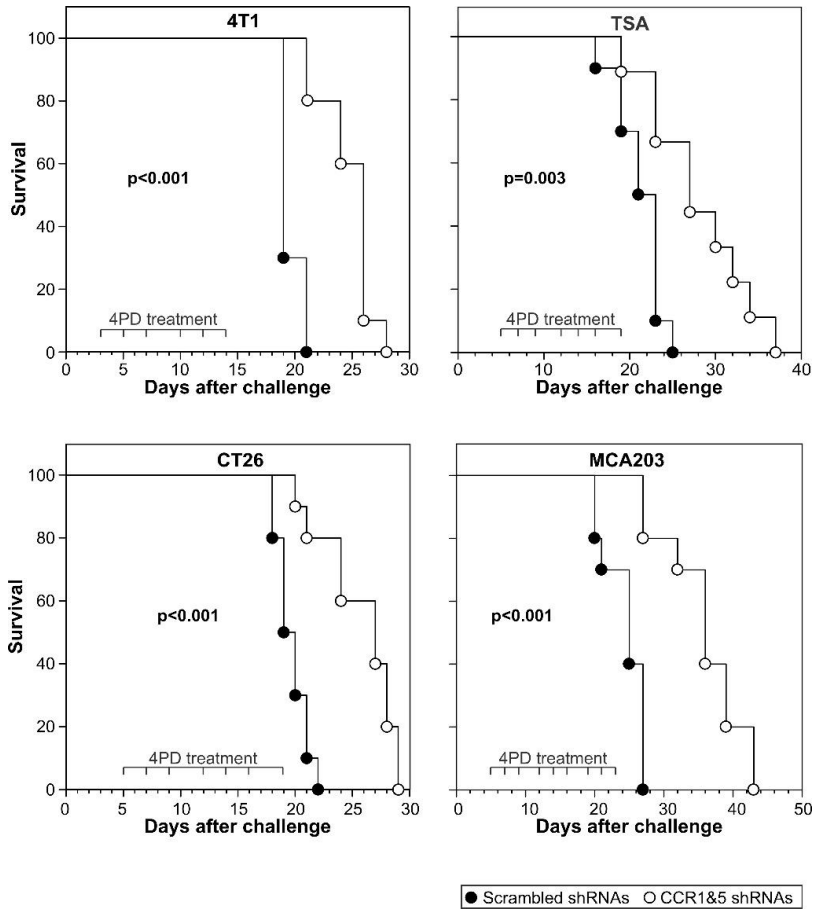

Supplemental figure 2: CCR1 and CCR5 targeted silencing delays tumor progression in multiple mouse models.

Mice (n=9-10) challenged with the indicated tumors were treated with 4PD conjugated with shRNAs specific for CCR1 and CCR5 or scrambled shRNAs once the tumors become palpable. Data derived from two independent experiments.

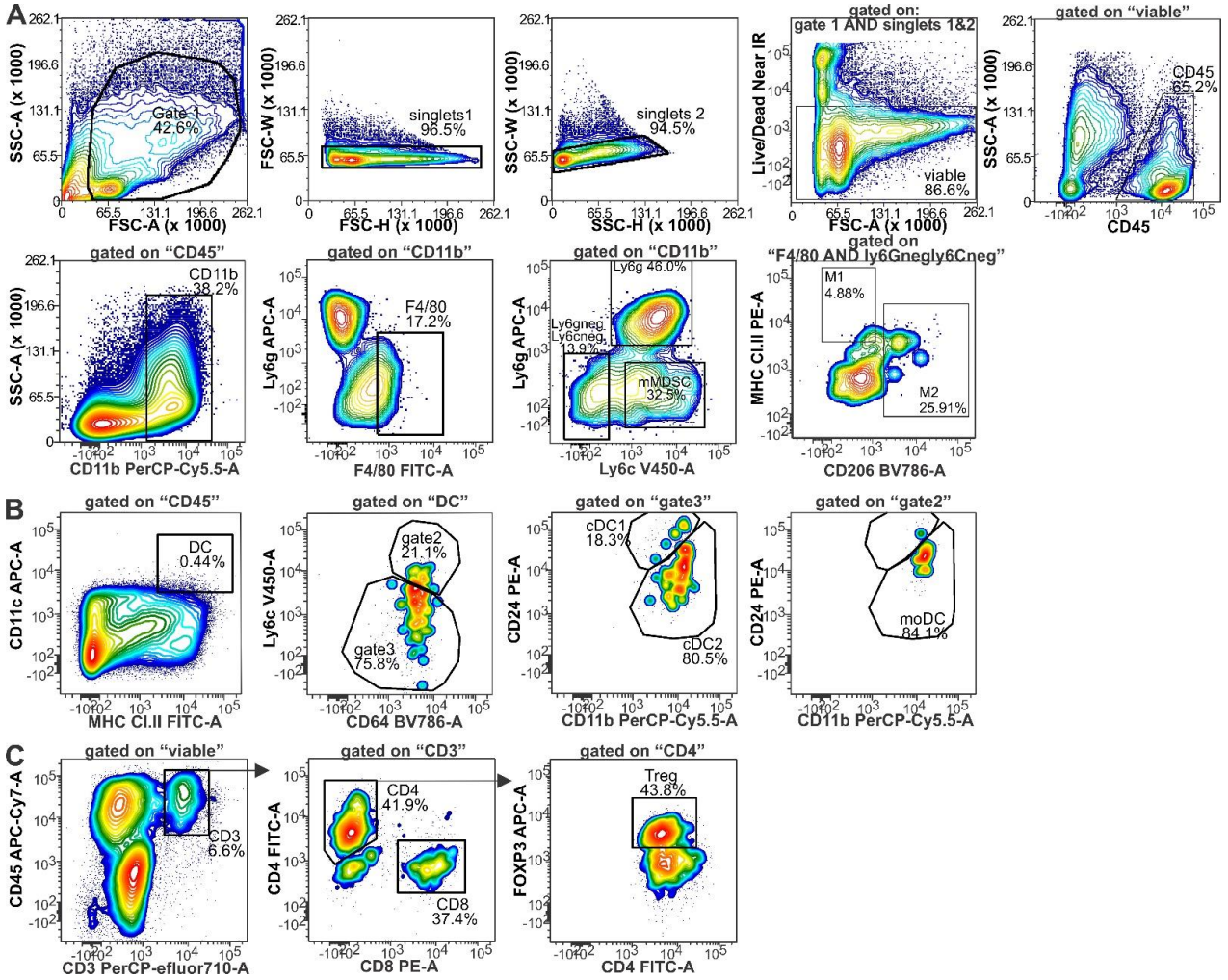

Supplemental figure 3. Gating strategy for myeloid (A), DCs (B), or T cells (C) subsets is shown and based on FMO controls.

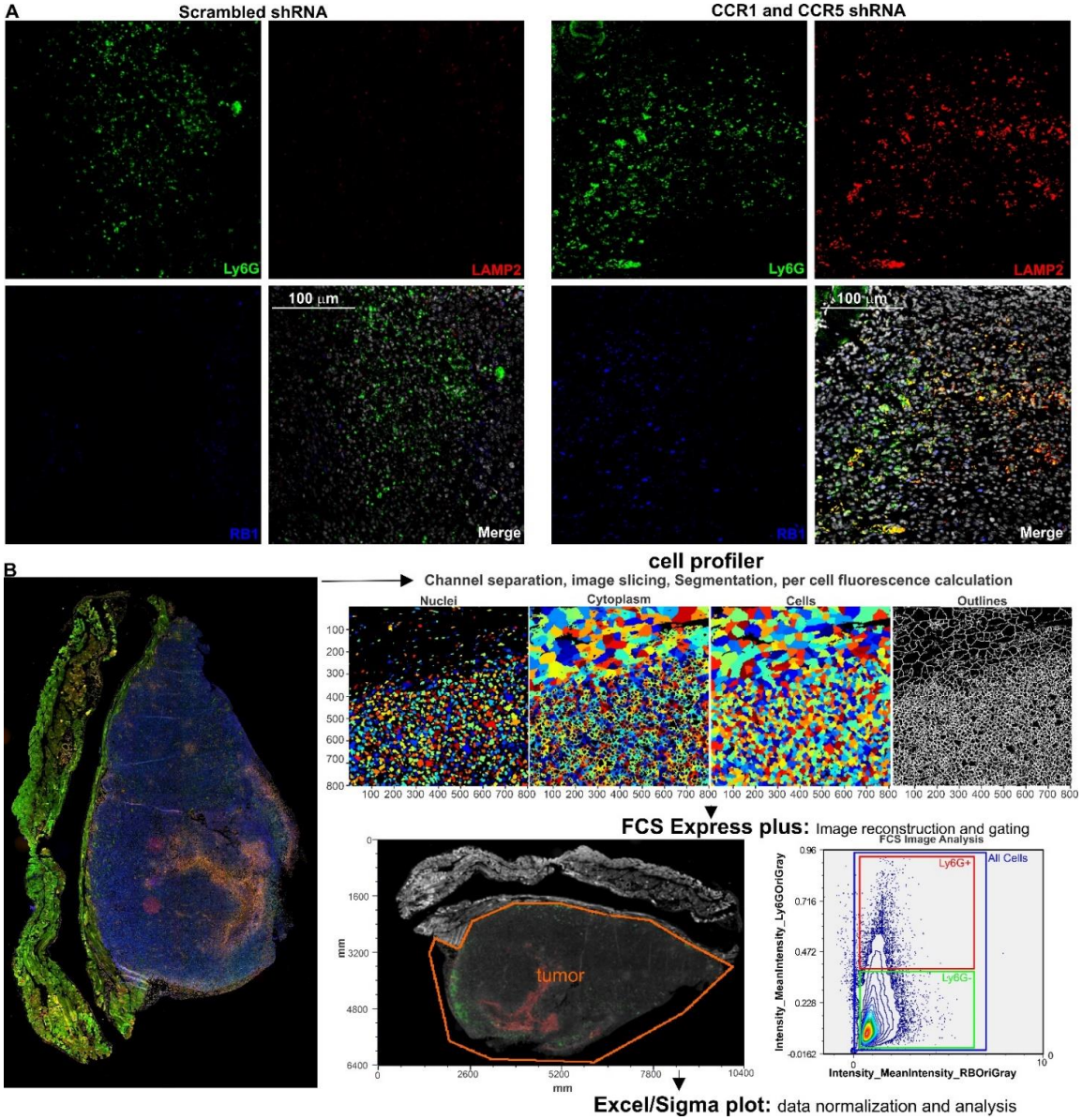

Supplemental figure 4: CCR1 and CCR5 silencing upregulated RB1 and LAMP2 in tumor infiltrating polymorphonucleate cells. 4T1 tumors from mice treated with scrambled shRNAs or CCR1 and CCR5 shRNAs were stained with DAPI and antibodies against Ly6G, RB1, and LAMP2. **B)** Scanned images from each channel of whole tumor sections were sliced in 500x500 pixel images using totalImageSlicer (https://www.coolutils.com/) and fed into cellprofiler as 8bit gray images. Primary objects (nuclei) were identified using the DAPI channel with a nuclei diameter set between 2 and 8 pixels, using the three classes Otsu Adaptive threshold method with a correction factor of 1 and the lower and upper bounds on threshold 0.1–1.0. Clumped objects were distinguished by shape and the size of the smoothing filter and minimum allowed distance between local maxima were automatically calculated. Secondary objects were identified using the autofluorescence and fluorescence of the merged image from the 3 channels acquired using the nuclei propagation method with three-classes Otzu Adaptive threshold method, 0.9 as threshold correction factor (0.0–1.0 range) and 0.02 as regularization factor. The cytoplasm as tertiary object was define as cell (secondary object) area minus the nuclei (primary object) area. For each cell, the integrated intensity mean of the DAPI channel in the nuclei and the integrated intensity mean of the Ly6G, RB1, and Ly6G channels in the cells were exported as .cpout file and analyzed using FCS Express PLUS vs7. A "tumor" gate/ROI was drawn to delineate the tumor area identified in H&E serial sections and RB1 and LAMP2 expression was evaluated within the intratumoral Ly6G$^+$ and Ly6G$^-$cells. Data were normalized to the background (all cells gate) median intensity.

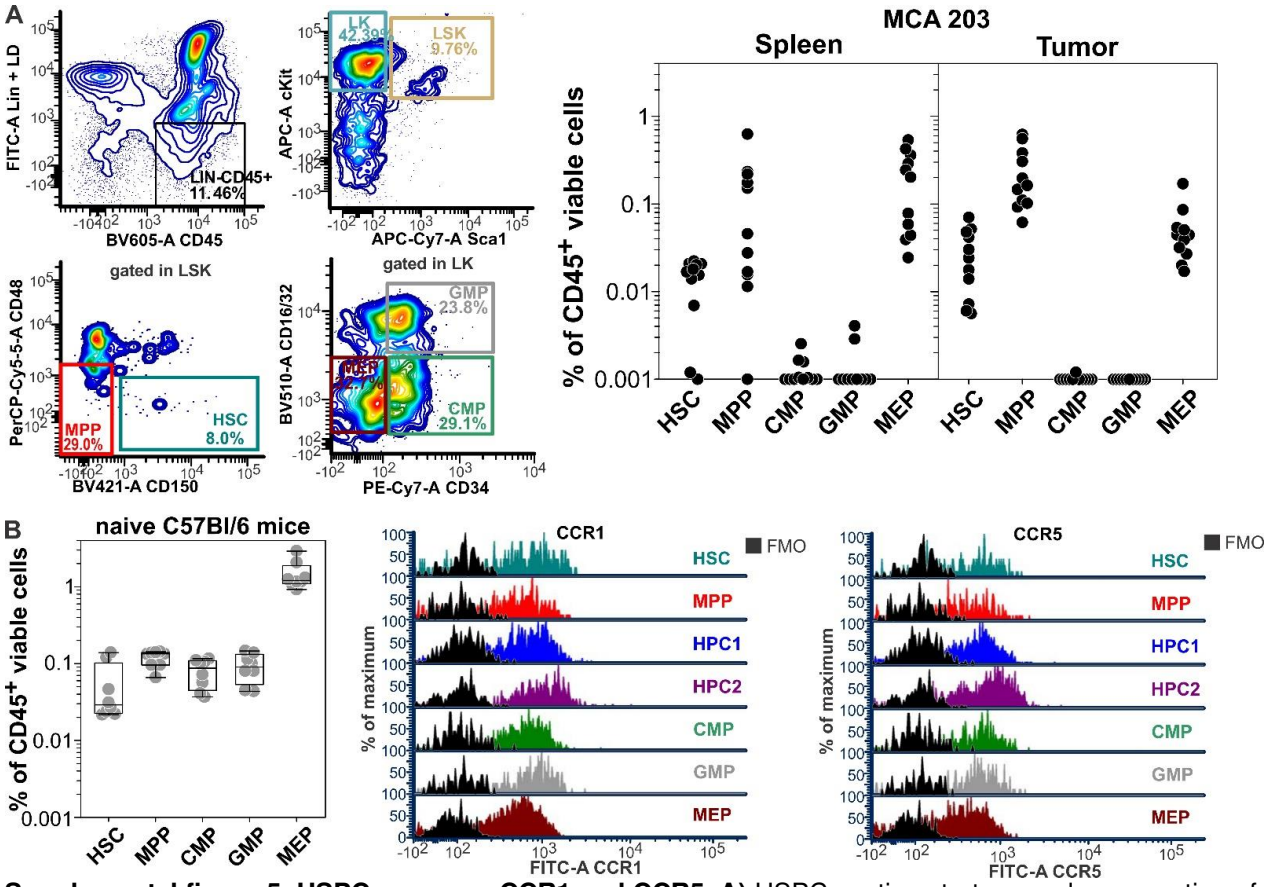

Supplemental figure 5: HSPCs express CCR1 and CCR5. A) HSPCs gating strategy and enumeration of HSPC subsets in the spleens and tumors (~0.5 cm of diameter) of mice bearing the MCA203 fibrosarcoma. **B)** Expression of CCR1 and CCR5 in the HSPC subsets from the bone marrow of naïve C57BL/6**.**

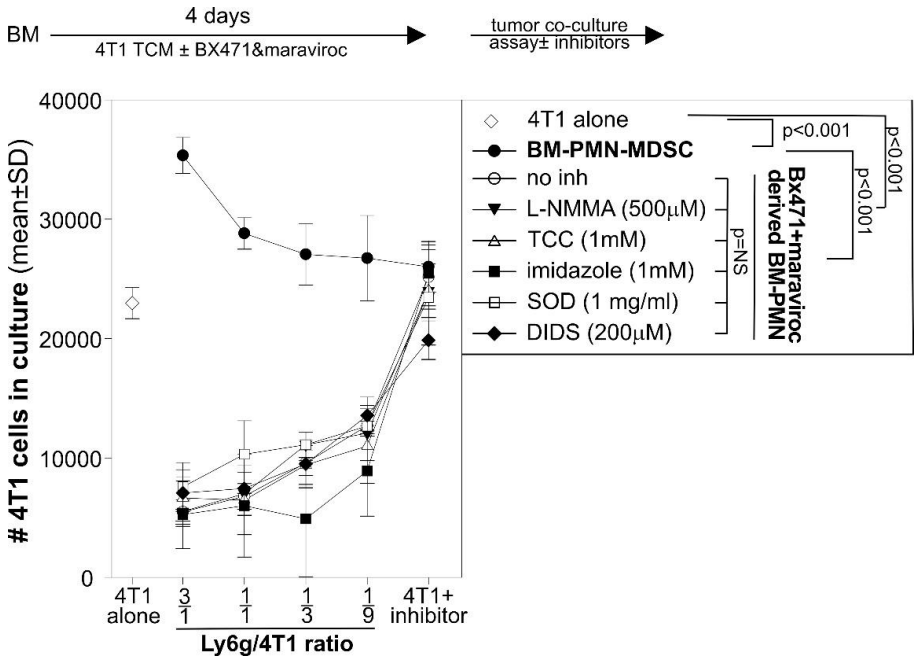

Supplemental figure 6: The main pathways involved in neutrophil cytotoxicity do not appears to mediate the observed tumoricidal activity. BM cells from naïve Balb/C mice were cultured for 4 days with 4T1-TCM in the presence or in the absence of Bx471 and Maraviroc. Flow cytometry analysis revealed that more than 90% of cells were $CD11b^{+}Ly6G^{+}$ in the "TCM + antagonists" group. $CD11b^{+}$cells were magnetically purified and cultured with 4T1-luc cells at the indicated ratio in the presence of the indicated inhibitor or vehicle. 18 hours later the number of tumor cells was determined by luciferase assay. Commercially available inhibitors were used at the reported relevant concentration. Specifically, L-NMMA was used to inhibit nitric oxide synthase 2 as in [29], N,N',N''-Triacetylchitotriose (TCC) to inhibit lysozyme as in[30], imidazole to inhibit the respiratory burst as in [31], superoxide dismutase (SOD) to inhibit superoxide action as in[32]; and 4,4′-Diisothiocyanatostil-bene-2,2′-disulfonic acid disodium salt (DIDS) to inhibit degranulation and NETosis as in[33].

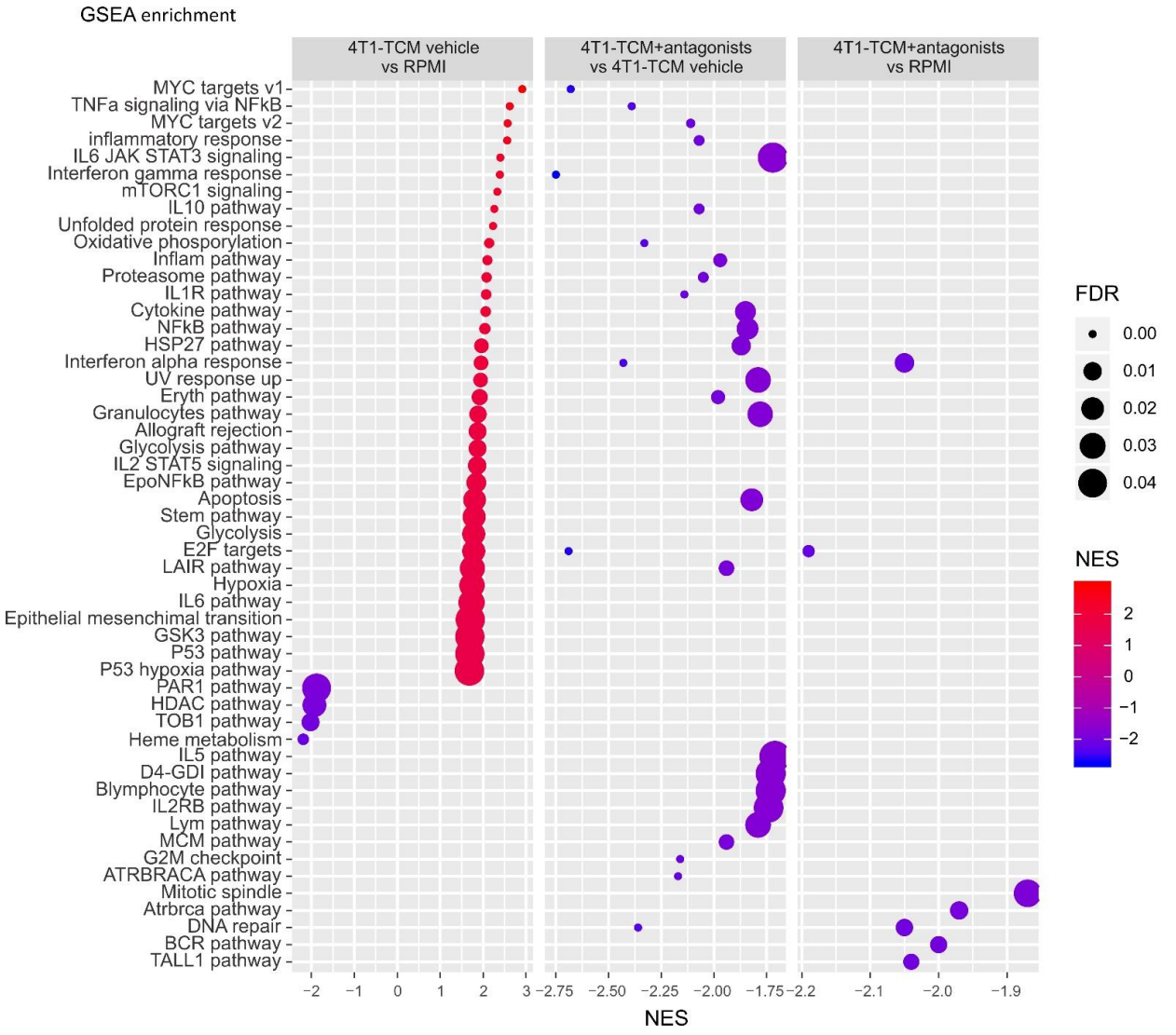

Supplementary figure 7: CCR1 and CCR5 blockade during MDSC differentiation inhibits the MDSC pathways upregulated by tumor derived factors. GSEA enrichment analysis was performed on the microarray data comparing: i) BM cells stimulated with 4T1-TCM (4T1) or complete media (RPMI), ii) BM cells stimulated with 4T1-TCM in the presence of Bx471 and Maraviroc (4T1+inhibitors) or in their absence, or iii) BM cells stimulated with 4T1-TCM in the presence of Bx471 and Maraviroc or cultured in complete media.

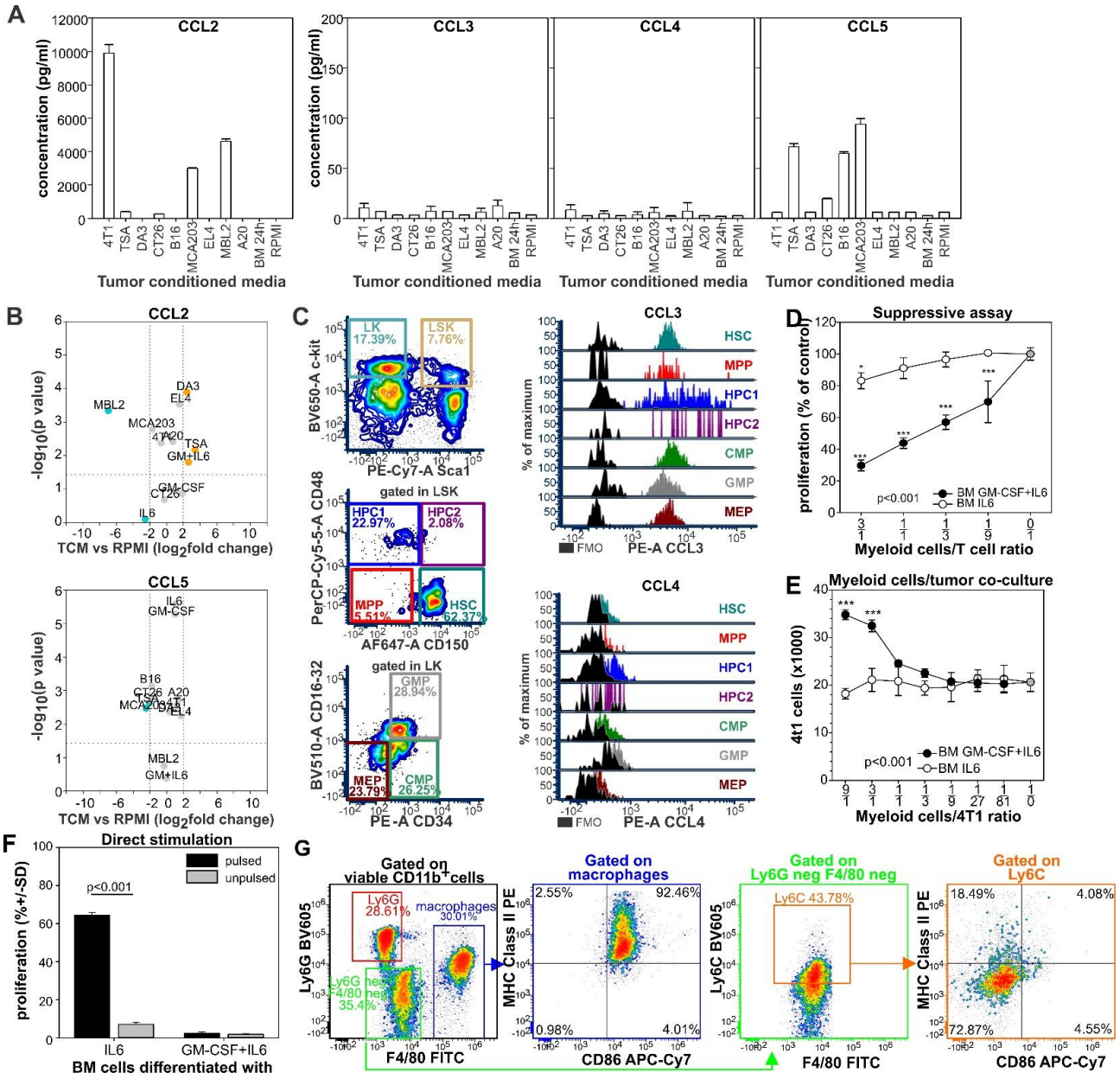

Supplemental figure 8: CCL2 and CCL5 are detectable in the TCM from different tumors but are poorly modulated in TCM stimulated BM cells whereas CCL3 and 4 are induced in different HSPC subsets.
A) CCL2, 3, 4 and 5 concentrations in the indicated tumor conditioned media were evaluated by Cytokine beads array. **B)** CCL2 and CCL5 concentrations were evaluated by cytokine beads arrays on BM cells stimulated for 24h by the indicated TCMs or indicated recombinant cytokines. The same TCMs incubated for 24h without BM cells were used as control. Supernatant from BM cells cultured in RPMI with no stimuli was used as negative control for the cultures with recombinant cytokines. Data derived from 2 independent experiments. **C)** HSPCs gating strategy and expression of CCL3 and CCL4 in BM cell subsets from C57BL/6 mice cultured for 4 hours with tumor conditioned media of the MCA203 fibrosarcoma cell line. **D, E, F)** BM cells from naïve Balb/c mice were cultured for 4 days with GM-CSF and IL6 or IL6 alone. $CD11b^+$cells were magnetically purified and **D)** tested in suppressive assays against HA specific CD8 cells stimulated with the relevant peptide; **E)** incubated with 4T1-luciferase cells for 18 hours; or **F)** pulsed with $HA_{518-526}$ peptide and incubated for 3 days with magnetically purified $CD8^+$HA-specific, CFSE-labeled T cells from Cl4 mice (pulsed myeloid cells/T cell ratio=3/1). Proliferation was evaluated by flow cytometry on viable $CD3^+CD8^+$cells. **G)** Flow cytometry analysis of Balb/C BM cells differentiated for 4 days by IL6 alone.

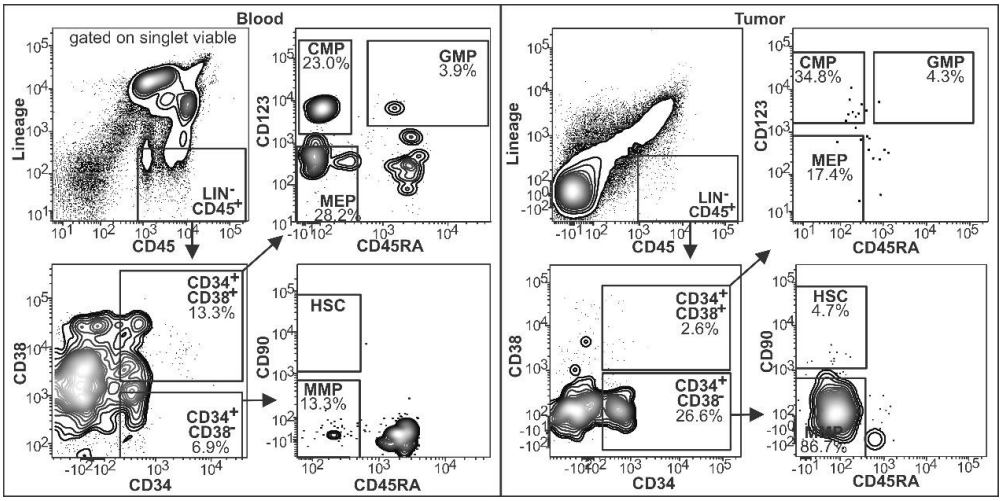

Supplemental figure 9: circulating HSPCs are present in patients with HNSCC. Gating strategy used for the enumeration of HSPCs in patients with HNSCC.

Supplemental references

1. Tusher VG, Tibshirani R, Chu G. Significance analysis of microarrays applied to the ionizing radiation response. Proc Natl Acad Sci U S A 2001;**98**(9):5116-21 doi: 10.1073/pnas.091062498.
2. Serafini P, Meckel K, Kelso M, et al. Phosphodiesterase-5 inhibition augments endogenous antitumor immunity by reducing myeloid-derived suppressor cell function. J Exp Med 2006;**203**(12):2691-702 doi: 10.1084/jem.20061104.
3. Pulaski BA, Ostrand-Rosenberg S. Mouse 4T1 breast tumor model. Curr Protoc Immunol 2001;**Chapter 20**:Unit 20 2 doi: 10.1002/0471142735.im2002s39.
4. Brattain MG, Strobel-Stevens J, Fine D, et al. Establishment of mouse colonic carcinoma cell lines with different metastatic properties. Cancer Res 1980;**40**(7):2142-6
5. Nanni P, de Giovanni C, Lollini PL, et al. TS/A: a new metastasizing cell line from a BALB/c spontaneous mammary adenocarcinoma. Clin Exp Metastasis 1983;**1**(4):373-80 doi: 10.1007/BF00121199.
6. Barth RJ, Jr., Bock SN, Mule JJ, et al. Unique murine tumor-associated antigens identified by tumor infiltrating lymphocytes. J Immunol 1990;**144**(4):1531-7
7. Bronte V, Cingarlini S, Apolloni E, et al. Effective genetic vaccination with a widely shared endogenous retroviral tumor antigen requires CD40 stimulation during tumor rejection phase. J Immunol 2003;**171**(12):6396-405 doi: 10.4049/jimmunol.171.12.6396.
8. Matory YL, Chen M, Dorfman DM, et al. Antitumor activity of three mouse mammary cancer cell lines after interferon-gamma gene transfection. Surgery 1995;**118**(2):251-5; discussion 55-6 doi: 10.1016/s0039-6060(05)80331-9.
9. Thomas GR, Chen Z, Oechsli MN, et al. Decreased expression of CD80 is a marker for increased tumorigenicity in a new murine model of oral squamous-cell carcinoma. International Journal of Cancer 1999;**82**(3):377-84 doi: 10.1002/(sici)1097-0215(19990730)82:3<377::Aid-ijc11>3.0.Co;2-9.
10. Kang Y, Siegel PM, Shu W, et al. A multigenic program mediating breast cancer metastasis to bone. Cancer Cell 2003;**3**(6):537-49 doi: 10.1016/s1535-6108(03)00132-6.
11. Gao JL, Wynn TA, Chang Y, et al. Impaired host defense, hematopoiesis, granulomatous inflammation and type 1-type 2 cytokine balance in mice lacking CC chemokine receptor 1. J Exp Med 1997;**185**(11):1959-68 doi: 10.1084/jem.185.11.1959.
12. Ishida N, Hayashi K, Hattori A, et al. CCR1 acts downstream of NFAT2 in osteoclastogenesis and enhances cell migration. J Bone Miner Res 2006;**21**(1):48-57 doi: 10.1359/JBMR.051001.
13. Leuschner F, Dutta P, Gorbatov R, et al. Therapeutic siRNA silencing in inflammatory monocytes in mice. Nat Biotechnol 2011;**29**(11):1005-10 doi: 10.1038/nbt.1989.
14. Kim SS, Peer D, Kumar P, et al. RNAi-mediated CCR5 silencing by LFA-1-targeted nanoparticles prevents HIV infection in BLT mice. Mol Ther 2010;**18**(2):370-6 doi: 10.1038/mt.2009.271.
15. Shields JD, Kourtis IC, Tomei AA, et al. Induction of lymphoidlike stroma and immune escape by tumors that express the chemokine CCL21. Science 2010;**328**(5979):749-52 doi: 10.1126/science.1185837.
16. Carpenter AE, Jones TR, Lamprecht MR, et al. CellProfiler: image analysis software for identifying and quantifying cell phenotypes. Genome Biol 2006;**7**(10):R100 doi: 10.1186/gb-2006-7-10-r100.
17. Schindelin J, Arganda-Carreras I, Frise E, et al. Fiji: an open-source platform for biological-image analysis. Nat Methods 2012;**9**(7):676-82 doi: 10.1038/nmeth.2019.
18. Bolstad BM, Irizarry RA, Astrand M, et al. A comparison of normalization methods for high density oligonucleotide array data based on variance and bias. Bioinformatics 2003;**19**(2):185-93 doi: 10.1093/bioinformatics/19.2.185.
19. Zilio S, Serafini P. Neutrophils and Granulocytic MDSC: The Janus God of Cancer Immunotherapy. Vaccines (Basel) 2016;**4**(3):31 doi: 10.3390/vaccines4030031.
20. Jablonski KA, Amici SA, Webb LM, et al. Novel Markers to Delineate Murine M1 and M2 Macrophages. PLoS One 2015;**10**(12):e0145342 doi: 10.1371/journal.pone.0145342.
21. Fridlender ZG, Sun J, Mishalian I, et al. Transcriptomic analysis comparing tumor-associated neutrophils with granulocytic myeloid-derived suppressor cells and normal neutrophils. PLoS One 2012;**7**(2):e31524 doi: 10.1371/journal.pone.0031524.
22. Youn JI, Collazo M, Shalova IN, et al. Characterization of the nature of granulocytic myeloid-derived suppressor cells in tumor-bearing mice. J Leukoc Biol 2012;**91**(1):167-81 doi: 10.1189/jlb.0311177.
23. Shaul ME, Levy L, Sun J, et al. Tumor-associated neutrophils display a distinct N1 profile following TGFbeta modulation: A transcriptomics analysis of pro- vs. antitumor TANs. Oncoimmunology 2016;**5**(11):e1232221 doi: 10.1080/2162402X.2016.1232221.

24. Lu C, Redd PS, Lee JR, et al. The expression profiles and regulation of PD-L1 in tumor-induced myeloid-derived suppressor cells. Oncoimmunology 2016;**5**(12):e1247135 doi: 10.1080/2162402X.2016.1247135.
25. Sica A, Bronte V. Altered macrophage differentiation and immune dysfunction in tumor development. J Clin Invest 2007;**117**(5):1155-66 doi: 10.1172/JCI31422.
26. Ko J, Rayman PA, Yang Y, et al. Differential gene expression in G-MDSC and neutrophils from renal cell carcinoma patients. Journal for ImmunoTherapy of Cancer 2014;**2**(S3):P216-P16 doi: 10.1186/2051-1426-2-s3-p216.
27. Zhou J, Nefedova Y, Lei A, et al. Neutrophils and PMN-MDSC: Their biological role and interaction with stromal cells. Semin Immunol 2018;**35**:19-28 doi: 10.1016/j.smim.2017.12.004.
28. Elpek KG, Cremasco V, Shen H, et al. The tumor microenvironment shapes lineage, transcriptional, and functional diversity of infiltrating myeloid cells. Cancer Immunol Res 2014;**2**(7):655-67 doi: 10.1158/2326-6066.CIR-13-0209.
29. Bronte V, Serafini P, De Santo C, et al. IL-4-induced arginase 1 suppresses alloreactive T cells in tumor-bearing mice. J Immunol 2003;**170**(1):270-8 doi: 10.4049/jimmunol.170.1.270.
30. Attri P, Kaushik NK, Kaushik N, et al. Plasma treatment causes structural modifications in lysozyme, and increases cytotoxicity towards cancer cells. Int J Biol Macromol 2021;**182**:1724-36 doi: 10.1016/j.ijbiomac.2021.05.146.
31. Kantar A, Oggiano N, Gabbianelli R, et al. Effect of Imidazole Salicylate on the Respiratory Burst of Polymorphonuclear Leukocytes. Current Therapeutic Research-Clinical and Experimental 1993;**54**(2):241-47 doi: Doi 10.1016/S0011-393x(05)80607-1.
32. Bowler RP, Nicks M, Tran K, et al. Extracellular superoxide dismutase attenuates lipopolysaccharide-induced neutrophilic inflammation. Am J Respir Cell Mol Biol 2004;**31**(4):432-9 doi: 10.1165/rcmb.2004-0057OC.
33. Maueroder C, Mahajan A, Paulus S, et al. Menage-a-Trois: The Ratio of Bicarbonate to CO2 and the pH Regulate the Capacity of Neutrophils to Form NETs. Front Immunol 2016;**7**(583):583 doi: 10.3389/fimmu.2016.00583.

CCR1 and CCR5 mediate cancer driven myelopoiesis and MDSC differentiation.

Serena Zilio, Silvio Bicciato, Donald Weed, and Paolo Serafini

Graphical Abstract

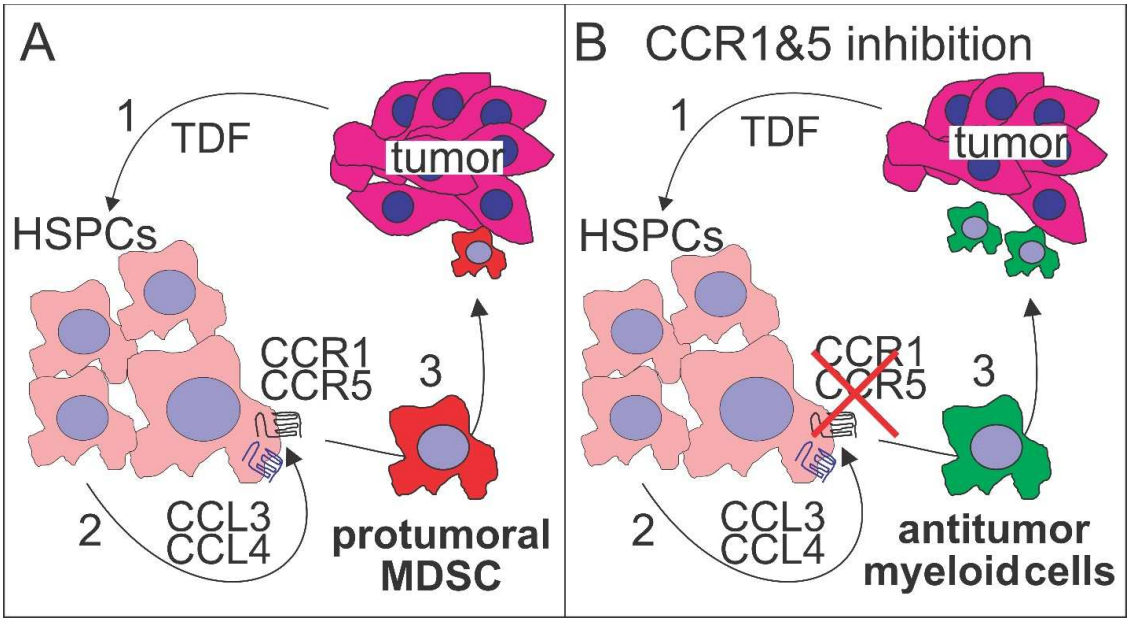

A) Tumor derived factors (1) induce HSPCs to upregulate and secrete of CCL3 and CCL4 (2). These chemokines autocrinally bind to CCR1 and CCR5 and activate their differentiation into MDSCs (3) favoring tumor progression and metastasis. **B)** Inhibition of CCR1 and CCR5 signaling blocks HSPCs conversion in MDSCs, restores the default differentiation of myeloid cells with anti-tumor activity, and reduces tumor progression.